Evidence for the evolution of eusociality in stem ants and a systematic revision of † Gerontoformica (Hymenoptera: Formicidae)

Zoological Journal of the Linnean Society, This is an Open Acc, **XX**, 1–35. With 17 figures.

Evidence for the evolution of eusociality in stem ants and a systematic revision of †*Gerontoformica* (Hymenoptera: Formicidae)

BRENDON E. BOUDINOT[1,*], ADRIAN RICHTER[1], JULIAN KATZKE[2], JÚLIO C. M. CHAUL[3], ROBERTO A. KELLER[2,4], EVAN P. ECONOMO[2], ROLF GEORG BEUTEL[1] and SHÛHEI YAMAMOTO[5]

[1]*Institut für Zoologie und Evolutionsforschung, Friedrich-Schiller-Universität Jena, Erberstraße 1, 07743 Jena, Germany*
[2]*Biodiversity and Biocomplexity Unit, Okinawa Institute of Science and Technology Graduate University, Onna, Japan*
[3]*Pós-Graduação em Ecologia, Departamento de Biologia Geral, Universidade Federal do Viçosa, 36570-900, Viçosa, Minas Gerais, Brazil*
[4]*Museu Nacional de História Natural e da Ciência & cE3c, Faculdade de Ciências da Universidade de Lisboa, 1749-016 Lisbon, Portugal*
[5]*Hokkaido University Museum, Hokkaido University, Kita 8, Nishi 5, Kita-ku, Sapporo 060-0808, Japan*

Received 3 July 2021; revised 1 October 2021; accepted for publication 8 October 2021

It is generally assumed that Cretaceous stem ants were obligately eusocial, because of the presence of wingless adult females, yet the available evidence is ambiguous. Here, we report the syninclusion of a pupa and adult of a stem ant species from Mid-Cretaceous amber. As brood are immobile, the pupa was likely to have been transported by an adult. Therefore, the fossil substantiates the hypothesis that wingless females were cooperators, thus these were true 'workers'. Re-examination of all described Cretaceous ant species reveals that winged–wingless diphenism – hence a variable dispersal capacity – may have been ancestral to the total clade of the ants, and that highly specialized worker-specific phenotypes evolved in parallel between the stem and crown groups. The soft-tissue preservation of the fossil is exceptional, demonstrating the possibility of analysing the development of the internal anatomy in stem ants. Based on the highest-resolution µ-CT scans of stem ants to date, we describe †***Gerontoformica sternorhabda* sp. nov.**, redescribe †*G. gracilis*, redefine the species group classification of †*Gerontoformica*, and provide a key to the species of the genus. Our work clarifies the species boundaries of †*Gerontoformica* and renders fossils relevant to the discussion of eusocial evolution in a way that has heretofore been intractable.

ADDITIONAL KEYWORDS: micro-computed tomography – palaeontology – phenotypic plasticity – sociobiology – taxonomy.

INTRODUCTION

Ants are exceptional among animals in that all 13 000+ of their extant species are obligately eusocial or are specialized social parasites, and no facultatively or primitively eusocial intermediates have survived to the present day. It is generally thought that ants crossed the morphological threshold to superorganismality by the Mid-Cretaceous, i.e. to have derived by then (female) castes that are anatomically distinct and have unequal reproductive potential. This conclusion is based on the assumptions that wingless female stem ants are morphologically differentiated workers, and that aggregations of these females represent sibling nestmates. However, the present evidence along these

*Corresponding author. Email: boudinotb@gmail.com
[Version of record, published online 5 February 2022; http://zoobank.org/ urn:lsid:zoobank.org:pub:0BE2F196-846F-4AD2-8C4D-79639B7E409C]

lines is insufficient to support this claim, as it has yet to be demonstrated that stem ants displayed the keystone of social organization: cooperation.

Stem ants, i.e. those extinct lineages that do not belong to the extant (crown) clade of Formicidae, are known from the Mid- to Late Cretaceous, with a described diversity from amber of 48 species attributed to 22 genera in six primary subgroups (Boudinot *et al.*, 2020a, b). The minimum age for obligate eusociality in ants is the Turonian (94–90 Mya) based on a single crown group fossil from New Jersey (Raritan) amber (Grimaldi & Agosti, 2000). A more diverse range of crown subfamilies have been recovered from the Late Campanian (84–71 Mya) via Canadian (Grassy Lake) and Burmese (Tilin) ambers (Dlussky, 1999; Engel & Grimaldi, 2005; McKellar *et al.*, 2013; Zheng *et al.*, 2018). No ants, stem or crown, have been discovered between the end of the Campanian and the End Cretaceous mass extinction event, and no stem Formicidae have been recovered in Cenozoic fossil deposits (LaPolla *et al.*, 2013; Barden, 2017; Boudinot *et al.*, 2020b). From their geological occurrences alone, stem ants certainly overlapped with crown ants for at least 20 million years, although possibly much longer given variation in divergence dating results for the extant fauna (reviewed in Borowiec *et al.*, 2020).

For stem ants, the strongest available evidence for obligate eusociality comprises the putative winged ('queen') and wingless ('worker') pairs of †*Zigrasimecia* Barden & Grimaldi, 2013 and certain species of †Haidomyrmecinae (Perrichot *et al.*, 2008, 2020; Cao *et al.*, 2020c; Guo *et al.*, 2021). These fossils suggest that stem ants had developmentally differentiated castes (Wheeler, 1986; Khila & Abouheif, 2010), which is arguably the key marker for the major transition to superorganismality (Wheeler, 1986; Boomsma & Gawne, 2018). However, dispersal polymorphisms are widespread among non-social insects, which can vary from macroptery to complete aptery, with winged–wingless diphenism occurring in lineages across the hemimetabolous and holometabolous orders. Such variability is more closely associated with environmental rather than social pressures (e.g. Rolf, 1990; Wagner & Liebherr, 1992), despite recent arguments that dispersal polymorphism is more important for eusocial origins than monogamy and kin selection (Nowak *et al.*, 2010). Moreover, the evolution of winglessness in ants is uninformative for social derivation on its own, as flightlessness has evolved repeatedly throughout many lineages of non-social Hymenoptera (Hanna & Abouheif, 2021), including 'Symphyta', 'Parasitica' and non-ant Aculeata.

The only other material evidence available for the inference of obligate eusociality in stem ants comprises syninclusions (co-preserved individuals) of wingless females, the putative nestmates of the genera †*Gerontoformica* Nel & Perrault, 2004 and †*Zigrasimecia* (Barden & Grimaldi, 2016; Cao *et al.*, 2020b). However, these fossils do not necessarily imply cooperation, because aggregations are observed with some frequency in non-social insects captured in mass emergence, sexual congregation, or various other forms of mass mortality (e.g. Batelka *et al.*, 2011; Peris & Jelínek, 2020; Storari *et al.*, 2021); aggregations may also be due to transport and deposition prior to fossilization (e.g. Heggen *et al.*, 2012). Indeed, the opposite of cooperation has been preserved by just such wingless female syninclusions, specifically through conflict in the form of aggression or combat among stem ants (Barden & Grimaldi, 2016; B. E. B., pers. obs.). Taken together, the available evidence for obligate eusociality in stem ants is strongly suggestive, but the puzzle remains incomplete.

It is in this context that we report the first fossil evincing cooperation for a stem ant species, via a syninclued adult–pupa pair of wingless female †*Gerontoformica*. Because more than one species of ant was preserved in this amber piece, we conducted detailed anatomical study based on photomicrography and the highest resolution micro-computed tomography (μ-CT) scans of stem ants to date. During this process, we found that it was necessary to systematically revise the ant genus †*Gerontoformica*, which we augmented by direct stereomicroscopic examination of type and non-type specimens. To understand the potential for reproductive division of labour among stem groups, we also reviewed the complete fossil record of described Mesozoic ants. Overall, our objectives are to consolidate the evidence of eusocial evolution among stem ants, and to provide a template for future studies of fossil Formicidae.

MATERIAL AND METHODS

Material

The focal amber piece originated from a deposit in the Hukawng Valley, Kachin State, northern Myanmar, dated near the Albian–Cenomanian boundary (Mao *et al.*, 2018), but perhaps older (Balashov, 2021). This formation has recently yielded a number of interesting insect fossils (e.g. Gustafson *et al.*, 2020: Shi *et al.*, 2020; Giłka *et al.*, 2021; Hsiao *et al.*, 2021; Jouault *et al.*, 2021a, b; Wu *et al.*, 2021).

The fossil itself is a relatively large piece of Kachin amber containing three wingless adult female ants plus a wingless pupa (Fig. 1); it is provided with the identification number AMNH Bu-SY23. The four syninclued ant specimens themselves were provided with unique specimen identifiers: CASENT0741231 (pupa) and CASENT0741232–CASENT0741234 (adults). To compare the anatomy of the pupa to

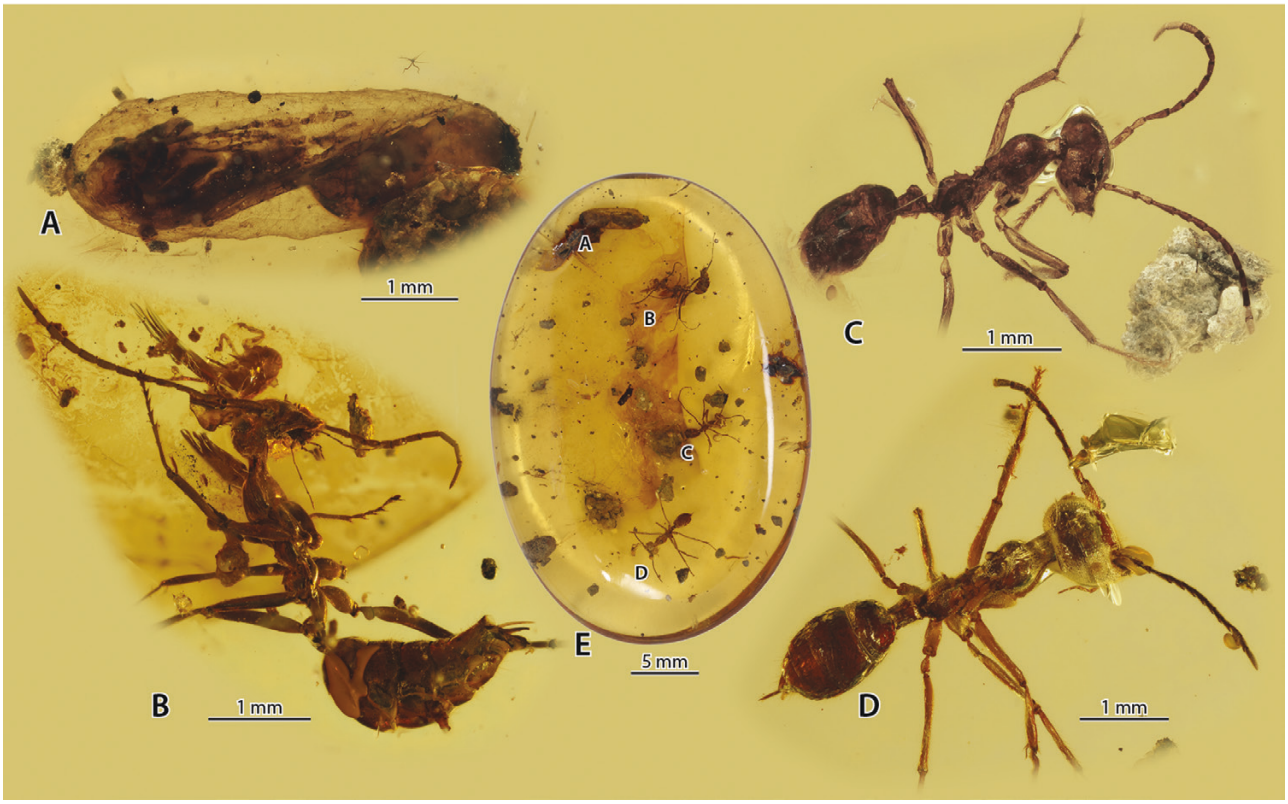

Figure 1. Overview of the Kachin amber piece and its syninclusions. A, the pupa of †*G. gracilis* (CASENT01741231). B, the adult of †*G. gracilis* (CASENT0741232). C, the holotype of †*G. sternorhabda* sp. nov. (CASENT0741233). D, the paratype of †*G. sternorhabda* sp. nov. (CASENT0741234). E, the entire amber piece (AMNH SY-23).

the workers for the purposes of identification, we performed photomicrography and μ-CT. Specimens of other stem Formicidae were directly examined from three collections: the American Museum of Natural History (AMNH), the Entomological Collection of the Coleoptera Laboratory, Viçosa, Brazil (CELC), and the research collection of Brendon E. Boudinot in Jena, Germany (BEBC).

Imaging, data processing and data availability

Photomicrographs were taken with a Canon EOS 80D digital camera with a Canon MP-E 65 mm macro lens (F2.8, 1–5 ×) and an attached Canon MT-24EX twin flash. Images were processed with Helicon Focus 7.5.4. Additional images were used from www.AntWeb.org under the Creative Commons 4.0 license.

The fossil was μ-CT scanned using a Zeiss Xradia 510 Versa 3D X-ray Microscope (Zeiss, Jena, Germany) operated with the Zeiss Scout-and-Scan Control System software (v.11.16411.17883) at the Okinawa Institute of Science and Technology Graduate University, Japan. We scanned the whole amber piece, the complete bodies for all adult workers and the pupa at varying magnifications, and the head and mesosoma of the best-preserved specimen (adult, CASENT074132), resulting in nine total scans. With the exception of the whole amber scan, the resultant voxel sizes ranged from 0.956 to 3.375 μm^3. For exposure times, source voltage, source power and other parameters, see Supporting Information, Fig. S1, Dataset 1.

A subset of the scans was segmented into regions of interest (ROIs) using Dragonfly 2020.1 (Object Research Systems, Montreal, Canada), with special attention to the head of the adult CASENT0741232, which displayed exceptional preservation. The ROIs were then used to mask copies of the original image data to extract specimens or individual structures and export them as .tif image stacks. The resultant segmented tiff files were rendered as Phong volumes using VG-Studio Max 3.4 (Volume Graphics GmbH, Heidelberg, Germany). Additionally, AMIRA 6.0 (Visage Imaging GmbH, Berlin, Germany) was used to export images of ortho-slices through the original image data of the CASENT0741232 head to show details of histological preservation.

The image plates were arranged in Adobe Photoshop CS6 (Adobe System Incorporated, San Jose, USA).

Labels were created in Adobe Illustrator CS6 (Adobe Systems Incorporated, San Jose, USA).

Scans of the specimens are available on Zenodo (doi:10.5281/zenodo.5608454).

Terminology

We employ the anatomical nomenclature of Richter *et al.* (2019, 2020, 2021) for the head, which we treat as if it were perfectly prognathous. For the mesosoma and metasoma, we follow Bolton (1994), Keller (2011) and Liu *et al.* (2018), with the exception that we do not recognize anapleural and katapleural regions, but upper and lower regions of the mesopectus and metapectus, respectively. Leg terms follow Boudinot (2015) for the coxae and trochanters, Bolton (1994, 2003) for the tibial spurs, and Beutel *et al.* (2020) for the tarsi and their anatomical elements. Following Boudinot *et al.* (2020b), we refer to thick traction setae as 'chaetae'. Finally, we apply the developmental character concept of Wagner (e.g. Wagner, 2014; McKenna *et al.*, 2021), i.e. that 'characters' are discrete anatomical entities and 'states' are continuous variations of those entities. Also note that two-letter abbreviations for genus names in †Haidomyrmecinae follow Boudinot *et al.* (2020b).

Species concept and criteria

We subscribe to the 'cohesion' species concept (Templeton, 1989; Barraclough, 2019), i.e. we conceive of species as populations or metapopulations that are reproductively independent (at least for non-clonal lineages), similar genetically and developmentally, and with distinct evolutionary trajectories. For the fossils considered in the present work, we pragmatically recognize the species criteria of diagnosability, phenetic clustering and apomorphy (*sensu* de Queiroz 1998, 2007). In other words, we expect individuals of fossil ant species to share discrete developmental characters, to share similar bodily proportions (i.e. developmental states), and that the strongest evidence for phylogenetic and evolutionary independence is synapomorphy. However, we do not consider synapomorphy to be sufficient alone, as paraphyletic (yet evolutionarily cohesive) species may be defined by plesiomorphies. Our reference for character polarity is Boudinot *et al.* (2020a). Because all known †*Gerontoformica* species are approximately co-eval in geological time, we are not concerned here with the effects of anagenesis on species delimitation.

Morphometrics

To clarify the species identity of the synincluded pupa, we took 38 linear measurements on the three-dimensional volume rendered surfaces of the specimens in VG-Studio Max. Use of the polyline length tool with the surface clipping function activated allowed us to set measurement points directly onto the specimen surface, resulting in straight line (2D) measurements contouring to the body between two (or more) points in 3D space. As not all body structures were perfectly preserved for all specimens, we selected ten informative measurements for further comparison (Measurement Definitions below), from which we also calculated three indices, i.e. ratios that represent body proportions (Index Definitions below). By calculating the differences in all measurements and indices between the three adult specimens and the pupa, we were able to determine average scores for the absolute value differences between them. For the absolute difference calculations and raw measurements, including all 38 measurements taken, see Supporting Information, Fig. S1, Dataset 1. All measurements are reported in mm and rounded to the nearest hundredths decimal place.

Measurement definitions

HWed	head width above eye (caudad) in full-face view.
HWev	head width below eye (orad) in full-face view.
EWl	minimum eye diameter, as taken from the left compound eye.
HD	head depth, i.e. the maximum distance from the face to the postgenal bridge of the head, as measured in profile view.
ML	mesosoma (Weber's) length, as measured in profile view from the inflection point between the pronotal neck and the pronotal disc to the middle point of the posterior surface of the propodeum.
PnLi	dorsomedian pronotum length, as measured from the inflection point to the middle point of the posterior pronotal margin.
PnWa	pronotum width, as measured across the dorsal inflection point of the pronotum, i.e. the posterodorsal inflection as seen in lateral view.
MnL	mesonotal length, or the maximum anterior to posterior length of the mesonotum.
AIIILm	first gastral tergum length, i.e. the length of the third abdominal tergum from the anterior inflection point between the helcium and posttergite to the posterior tergal margin.
AIIILl	first gastral segment height, i.e. distance from the posterior margin of the third abdominal sternum to the posterior margin of the third abdominal tergum along the midline of the body.

Index definitions

HPI	head proportion index: HD/HWed.
HSI	head size index: HWed/ML.
AIIILI	first gastral segment index: AIIILm/AIIILl.

Developmental characters

As a proxy for phenotypic differentiation among adult females, hence potential for reproductive division of labour, we evaluated the degree of polyphenism and morphological specialization of the mesosoma of stem ants. We considered the development of three focal structures for the wingless females of all described Mesozoic ants, where such females are known: (1) differentiation of the mesoscutum, or the anterior portion of the mesonotum, from the remainder of the mesosoma; (2) differentiation of the mesoscutellum or the smaller, posterior portion of the mesonotum; and (3) development of the metanotum. We chose these characters as they are: (1) the most consistent external feature of caste differentiation for ants, with exceptions (Peeters 2012); and (2) because mesosomal shape is highly variable across the Formicidae, with extreme worker-associated forms evolving numerous times across the phylogeny (e.g. Bolton 1994, 2003). We scored these characters as present (1) or absent (0), with inapplicable (–) recorded when wingless females are unknown. Note that we use the term 'worker-like' for all wingless individuals of stem ants that have some degree of flight sclerite reduction, and we use the phrase 'highly specialized wingless-specific or worker-like phenotypes' for individuals that have completely undifferentiated flight sclerites, i.e. those individuals scored 0 for characters 1–3.

In addition to AMNH, BEBC, CELC and AntWeb, we evaluated these characters from primary literature: †Armaniinae: Dlussky (1983, 1999); †*Haidomyrmex*: Cao *et al.* (2020a), Guo *et al.* (2021); †*Haidomyrmodes*: Perrichot *et al.* (2008); †*Haidoterminus*: McKellar *et al.* (2013); †*Linguamyrmex*: Miao *et al.* (2019), Barden *et al.* (2017); †*Orapia*: Dlussky *et al.* (2004). For raw data and further information, including excluded taxa and their references sources, see Supporting Information, Fig. S1, Dataset 2.

RESULTS

Identification

To identify the three adults preserved in the amber fossil, we evaluated qualitative characters at the genus (Boudinot *et al.*, 2020b), species group (Boudinot *et al.*, 2020b) and species level (Barden & Grimaldi, 2014). The specimens were identifiable as †*Gerontoformica* (Nel *et al.*, 2004) by the simple, bidentate mandibles (Figs 2K, 7C), the posterior margin of the clypeus, which does not extend aborally between the antenna toruli (Fig. 2K, L), and the anterior margin of the clypeus which is not produced anteriorly as a lobate process (Fig. 2K, L). Based on further qualitative characteristics outlined below, it was apparent that the adults represent two species that were captured in absolute sympatry.

The adult specimen CASENT0741232 (C-32) was determined to be a member of the †*G. gracilis* (Barden & Grimaldi, 2014) species group due to absence of a constriction on abdominal tergite and sternite IV (metasomal III) (Figs 2B, 7B), in addition to absence of a transverse ridge dividing the mesonotum into distinct mesoscutal and mesoscutellar regions (Fig. 2E). Of all described species in the *G. gracilis* group, C-32 specifically resembles †*G. gracilis* in having a relatively thin and long mesothorax and a poorly developed subpetiolar process (Fig. 2B). No further distinguishing features were found; thus, we consider C-32 to be conspecific with †*G. gracilis*.

The adult specimens CASENT0741233 and CASENT074134 (C-33, C-34) were determined to be members of the †*G. pilosa* (Barden & Grimaldi, 2014) species group due to presence of the abdominal segment IV constriction and the transverse mesonotal ridge (Figs 2C, 4C, F). Among all †*G. pilosa* group species, these two specimens are most similar to †*G. pilosa* itself due to their comparatively less robust mesosomata than †*G. contegus* (Barden & Grimaldi, 2014) and †*G. magnus* (Barden & Grimaldi, 2014). However, they differ from †*G. pilosa* in having a distinctly digitate subpetiolar process (Fig. 2C) and an anteroposteriorly narrower prora (the anteroventrally situated process of abdominal segment III/ metasomal II) (Fig. 2C). For these reasons, we consider C-33 and C-34 to represent an undescribed species near †*G. pilosa*. See the diagnosis of the new species, †*G. sternorhabda*, below for more fine-grained distinctions.

We consider the pupa to be a representative of †*G gracilis* because, on average, the morphometrics of the pupa were > 2× more similar to those of specimen C-32 than either specimens C-33 or C-34. Although a number of structures are incompletely developed, the pupa shares a set of distinct features with specimen C-32 to the exclusion of C-33 and C-34: (1) their heads are anteroposteriorly longer than lateromedially broad (Fig. 2J, K; vs. broader than long, Fig. 2L); (2) their maxillary palps are six-merous (Fig. 7; vs. five-merous; see note 5 of the description of †*G. sternorhabda*); (3) their pronota are longer than tall in lateral view (Fig. 10; vs. about as long as tall, Fig. 5); and (4) their mesonota are evenly rounded in lateral view (Fig. 10; vs. angled, Fig. 5).

Female diphenism and specialization

In total, we were able to score mesosomal development for 48 of the 64 species-level taxa attributed to the stem Formicidae, with the total count including impression fossils (Supporting Information, Fig. S1, Dataset 1, summarized in Fig. 3A). Those taxa that

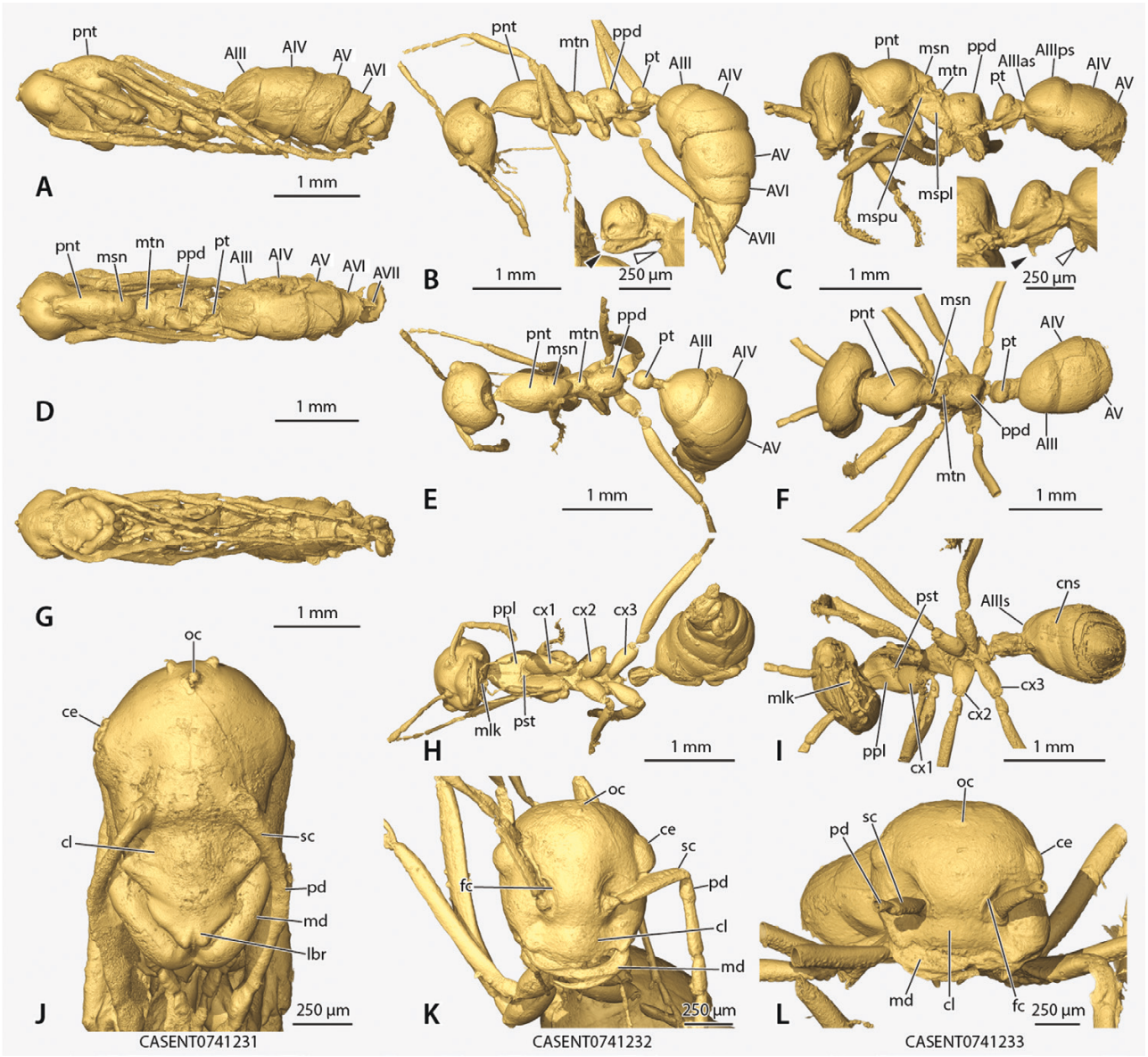

Figure 2. Volume renders of the pupa and two of the adult specimens. The black arrows indicate the subpetiolar process, while the white arrows indicate the prora. A–C, lateral view. D–F, dorsal view. G–I, ventral view. J–L, facial view. A, D, G, J. the pupa of †*G. gracilis*. B, E, H, K, the adult of †*G. gracilis*. C, F, I, L, the holotype of †*G. sternorhabda* sp. nov.. Abbreviations: AIII–VII, third through seventh abdominal segments; AIIIas, anterior surface of third abdominal segment; AIIIps, posterior surface of third abdominal segment; ce, compound eye; cl, clypeus; fc, frontal carina; lbr, labrum; md, mandible; msn, mesonotum; mspl, lower mesopectal region; mspu, upper mesopectal region; mtn, metanotum; oc, ocellus; pd, pedicel; pnt, pronotum; ppd, propodeum; pst, prosternum; pt, petiole; sc, scape.

were excluded were either known only from males or were of insufficient preservational quality to evaluate. Categorically, no wingless females are known for the †*Camelomecia* genus group or †Armaniinae, whereas the majority of other stem ant species are described from dealate or completely apterous individuals. The wingless genus †*Dolichomyrma* Dlussky, 1975, a putative Turonian armaniine, is recovered in the crown Formicidae in preliminary phylogenetic analysis (Boudinot *et al.*, 2020a). Therefore, these groups remain uninformative for the origin of female diphenism, depending on their formal phylogenetic placement.

All described species of †Haidomyrmecinae display discretely developed mesoscuta, mesoscutella and metanota (Fig. 3B), despite widespread occurrence of the dealate or apterous condition in this subfamily.

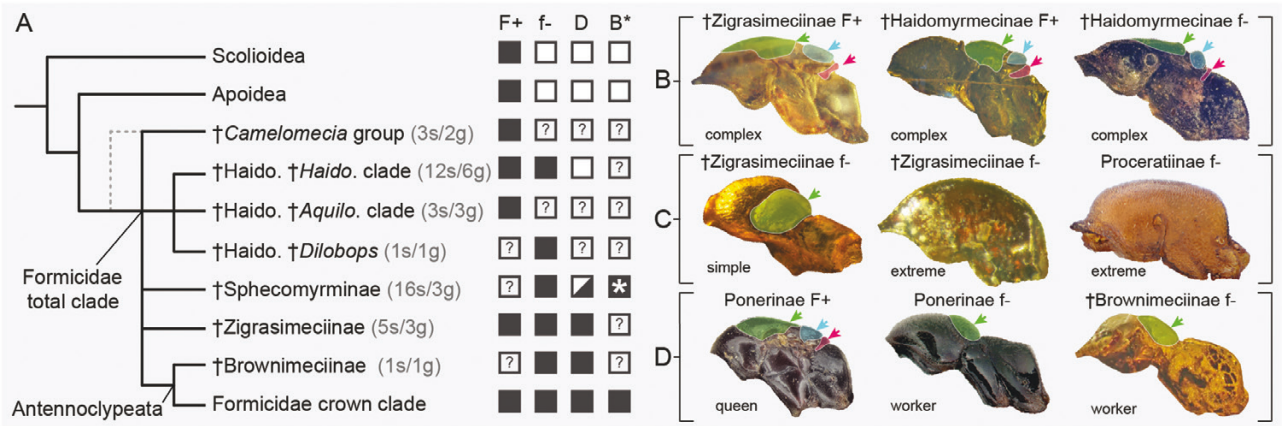

Figure 3. Summary of the evidence for eusocial evolution in stem groups. A, overview of the phylogenetic relationships of the total clade Formicidae, with key biological traits mapped. F+, winged females; f-, wingless females; D, developmental simplification of the mesosoma; and B*, brood care. Solid squares, trait confirmed as present; empty squares, trait confirmed as absent; half-filled squares, trait confirmed as variable; question marks, state uncertain; black square with asterisk, new evidence provided in the present study. B, exemplars of females with the full and complex complement of flight sclerites, namely the mesoscutum (green), mesoscutellum (blue), and metanotum (magenta). C, exemplars of wingless †Zigrasimeciinae demonstrating independent convergence on the extremely simplified mesosomal form of various crown Formicidae, illustrated in this case by *Discothyrea* (Proceratiinae). D, exemplars of the Antennoclypeata, showing a similar degree of sclerite reduction between †*Brownimecia* and crown Formicidae. *Notes*: The topology in 1A is summarized from Johnson *et al.* (2013), Barden & Grimaldi (2016) and Boudinot *et al.* (2020a). Images for rows 1B, C were downloaded from AntWeb (2021); taxon names, imagers and unique specimen identifiers are listed from left to right, top to bottom are as follows: †*Zigrasimecia tonsora* Barden & Grimaldi, 2013 (P. Barden, ANTWEB1008098); †*Dhagnathos autokrator* Perrichot *et al.*, 2020 (V. Perrichot, FANTWEB00022); †*Linguamyrmex rhinocerus* Miao & Wang, 2019 (V. Perrichot, FANTWEB00016); †*Protozigrasimecia chauli* Cao *et al.*, 2020c (H. Cao, FANTWEB00051); †*Zigrasimecia* ufv-01 (J. Chaul, ANTWEB10141055); *Discothyrea bobi* Chaul, 2020 (J. Chaul, UFV-LABECOL-000032); †*Brachyponera croceicornis* (Emery, 1900) (F. Esteves, CASENT0916594); *Brachyponera croceicornis* (Emery, 1900) (A. Nobile, CASENT0172432); †*Brownimecia clavata* Grimaldi *et al.*, 1997 (V. Perrichot, AMNH-NJ667).

However, †Haidomyrmecinae include the only species for which winged–wingless female pairs have been associated at the species level, namely †*Haidomyrmex cerberus* Dlussky, 1996 (see Guo *et al.*, 2021) †Haidomyrmodes *mammuthus* Perrichot *et al.*, 2008 and †*Linguamyrmex brevicornis* Perrichot *et al.*, 2020. No winged–wingless pairs of these species have been recovered in a syninclusion. Unfortunately, the wingless †*Hs. mammuthus* is broken at about the metathoracic region, but the mesoscutum and mesoscutellum are distinct in profile view. †*Linguamyrmex brevicornis* and †*Hx. cerberus*, on the other hand, appear to have discrete winged and wingless females, although the meso- and metanotal structures are still developed in the wingless individuals. The winged female †*Zigrasimecia* is of uncertain relationship to the presently described species (Cao *et al.*, 2020c), as is the alate-based putative new species described by Zhuang et al. (in press).

Among the other stem ants, the most variable state is expression of the mesoscutellum, which is differentiated in some but not all †Sphecomyrminae and is completely undifferentiated in †Zigrasimeciinae and †Brownimeciinae. In contrast, the metanotum is developed in all species except †*Brownimecia clavata* Grimaldi *et al.*, 1997, †*Myanmyrma maraudera* (Barden & Grimaldi, 2016) and †*Zigrasimecia*. The most extreme derivation of the mesosoma is observed in †*Zigrasimecia* (Fig. 3C), which has a completely fused and helmet-shaped mesosoma, similar in overall form to various crown Formicidae such as *Discothyrea* Roger, 1863 (Proceratiinae, Fig. 3C), *Tatuidris* Brown & Kempf, 1968 (Agroecomyrmecinae) or various Myrmicinae. Notably, †*Protozigrasimecia* Cao *et al.*, 2020 is intermediate, with a well-developed mesoscutum that has a free articulation with the pronotum (Fig. 3C). The form of †*Protozigrasimecia* and †*M. maraudera* (not shown) is also similar to †*Brownimecia* Grimaldi *et al.*, 1997, the sister-group to the crown ants (Barden & Grimaldi, 2016; Boudinot *et al.*, 2020a, b; Fig. 3D).

Systematic palaeontology

Family Formicidae Latreille, 1809

Subfamily †Sphecomyrminae Wilson & Brown, 1967

Genus †*Gerontoformica* Nel & Perrault, 2004

= †*Sphecomyrmodes* Engel & Grimaldi, 2005 junior syn.: Barden & Grimaldi (2016): 518.

TAXONOMIC SYNOPSIS OF †*GERONTOFORMICA*

I. Species group of *cretacica* (newly recognized) (*Charentese* amber) [Note 1]:

1. †*G. cretacica* Nel & Perrault, 2004 *nomen dubium* (new status) [Note 2] – Type species of †*Gerontoformica* Nel & Perrault, 2004
2. †*G. occidentalis* (Perrichot *et al.*, 2008)

II. Species group of *gracilis* (newly recognized) (*Kachin* amber):

3. †*G. gracilis* (Barden & Grimaldi, 2014)
4. †*G. robusta* (Barden & Grimaldi, 2014)
5. †*G. spiralis* (Barden & Grimaldi, 2014) [Note 3]
6. †*G. subcuspis* (Barden & Grimaldi, 2014) [Note 3]

III. Species group of *pilosa* (*Kachin* amber):

7. †*G. sternorhabda* sp. nov.
8. †*G. contega* (Barden & Grimaldi, 2014)
9. †*G. magna* (Barden & Grimaldi, 2014)
10. †*G. pilosa* (Barden & Grimaldi, 2014)

IV. *Incertae sedis* to species group within genus (*Kachin* amber):

(11.) †*G. orientalis* (Engel & Grimaldi, 2005) *nomen dubium* (new status) [Note 4] – Type species of †*Sphecomyrmodes* Engel & Grimaldi, 2005

(12.) †*G. rugosa* (Barden & Grimaldi, 2014) *nomen dubium* (new status) [Note 5]

(13.) †*G. tendir* (Barden & Grimaldi, 2014) *nomen dubium* (new status) [Notes 5, 6]

Notes on classification

Note 1: Under the label of '*orientalis* group', Boudinot *et al.* (2020b) previously united the *cretacica* and *gracilis* groups with the species †*G. orientalis*. The *cretacica* and *gracilis* groups are here divided based on the distinct forms of their petioles. The species †*G. orientalis* is of insufficient preservation for species-level identification (see Note 4 below).

Note 2: The holotype of †*Gerontoformica cretacica* is poorly preserved, as noted by Barden & Grimaldi (2016), with obvious distortions and elongation of the scapes and flagella, and little detail of the body visible. Due to this unfortunate circumstance, we newly consider †*G. cretacica* to be a *nomen dubium*. It remains in the *cretacica* species group of †*Gerontoformica,* because it is the type species of the genus. However, it will be highly desirable to clarify the identity of this species through examination and description of more Charentese ants. At present, the only distinction between †*G. cretacica* and the co-eval †*G. occidentalis* that is not apparently affected by preservation is body size, with the former having a longer mesosoma than the latter (2.1 mm vs. 1.4 mm, respectively). Body size is, of course, highly variable among nestmates of crown ants, thus is a weak diagnostic trait when used in isolation and without the quantification of variation across conspecific individuals.

Note 3: †*Gerontoformica spiralis* and †*G. subcuspis* were difficult to separate in the present study based on the available anatomical evidence and may be conspecific. Specifically, we observe that, in addition to conditions outlined in the key (see that section below), the two species are highly similar in the following conditions, which we only roughly characterize here: (1) proportions and fine details of the head, including frontal carina shape; (2) the degree of mesonotal, metanotal and propodeal convexity; (3) the width of separation between the meso- and metanota plus metanotum and propodeum; (4) the shape and proportions of the petiolar node; and (5) the form of the third abdominal (first 'gastral') segment. It is possible that †*G. spiralis* and †*G. subcuspis* represent the smaller and larger ranges of body size of a single species, with the former reported to have a total body length of 4.22–5.22 mm and the latter 5.35–5.76 mm (Barden & Grimaldi, 2014). Our focal uncertainties relate to the shapes and setational patterns of the tarsi of †*G. subcuspis*, and the form of the subpetiolar process and prora of †*G. spiralis*. A potential feature separating the two species is the distance of the toruli from the posterior clypeal margin, which appears to be narrower in †*G. spiralis* relative to †*G. subcuspis*, but this could be a visual artefact caused by the apparent light distortion in the holotype image of †*G. spiralis*. We recommend further re-evaluation of these two species, ideally using μ-CT and additional light photography to resolve the uncertainties of the tarsi, toruli and sternal processes of the metasoma. See also Note 1 on the diagnosis of †*G. gracilis*.

Note 4: †*Gerontoformica orientalis*, the type species of †*Sphecomyrmodes*, is identifiable as †*Gerontoformica* relative to †*Sphecomyrma* Wilson & Brown, 1967 by the absence of the anteromedian clypeal process and presence of traction setae/ chaetae along the anterior clypeal margin, as recognized in the original description (Engel & Grimaldi, 2005) and illustrated in Boudinot *et al.* (2020b). However, in †*Gerontoformica*, the species †*G. orientalis* is unidentifiable due to poor preservation. No details of the head are clearly observable, except for the antenna, mandibles and anterior clypeal margin, while the mesosoma appears

strongly distorted, the petiole is obscured, and the metasoma is mostly disarticulated. Boudinot *et al.* (2020b) placed †*G. orientalis* in the *orientalis* species group along with the type species of †*Gerontoformica* based on the absence of the cinctus of abdominal segment IV. As a more refined placement is not possible, we newly consider this species to be a *nomen dubium*.

Note 5: †*Gerontoformica rugosa* and †*G. tendir* are newly considered as *nomina dubia* due to their poor preservation, being strongly desiccated and thus distorted. Both species appear to have some degree of abdominal segment III petiolation, as observed in the three confirmed members of the *pilosa* group, but it cannot be determined whether this is natural or exaggerated due to preservation. It is possible, but not yet determinable, that †*G. rugosa* is conspecific with †*G. gracilis*. That †*G. rugosa* or †*G. tendir* do have sculptured integument remains possible but requires substantiation via additional material of these species. We note that little surface texture variation has been explicitly documented among stem ants thus far.

Note 6: †*Gerontoformica tendir* was defined by Barden & Grimaldi (2014) as having a medial clypeal lobe. This anteromedian lobe not only bears traction setae/chaetae, as previously observed, but is also lateromedially broader and proximodistally shorter than that of †*Sphecomyrma*. Given the poor preservation, it is possible that the apparent lobate form may be due to distortion of the amber matrix, as the lobe consists of the entire medial portion of the clypeus, which is distinct from the lateral clypeal lobes. Based on direct examination of the holotype, it appears that there is a transverse mesonotal carina in †*G. tendir*, but this also requires re-evaluation. Without additional specimens having an exaggerated and broadly, medially lobate clypeus, we remain uncertain about the identity of the species. A state of potential value for confirming the identity of †*G. tendir* from additional material is the absence of teeth on the pretarsal claws, as illustrated by Barden & Grimaldi (2014).

Remarks

The genus †*Gerontoformica* currently consists of 13 species, including the newly described †*G. sternorhabda*. The holotypes of nine of these species are sufficiently preserved for species-level identification, with eight of these being sufficiently defined given the potential synonymy of two (see Note 3 above). At the generic level, †*Gerontoformica* differs from †*Sphecomyrma* by presence of traction setae/chaetae along the anterior clypeal margin and absence of a narrow anteromedian clypeal lobe. These two conditions were used by Engel & Grimaldi (2005) to establish the genus †*Sphecomyrmodes*, which was synonymized under †*Gerontoformica* by Barden & Grimaldi (2016) after examination of the holotype of the type species of the latter taxon. Collectively, †*Gerontoformica* and †*Sphecomyrmodes* have been revised piecemeal after the former's establishment by Nel *et al.* (2004). Specifically, Barden & Grimaldi (2014) added nine species of †*Sphecomyrmodes*, Barden & Grimaldi (2016) transferred all species of †*Sphecomyrmodes* to †*Gerontoformica*, and Boudinot *et al.* (2020b) moved one species to †*Myanmyrma* and recognized two morphologically defined groups of species in the genus.

To understand the shifting boundaries of †*Gerontoformica* in the light of the present µ-CT-driven study, we detail the species-level history of the genus. Species attributed to the genus are distributed in Kachin amber (11 total) and Charentese amber (two total). The Charentese species, †*G. cretacica* and †*G. occidentalis*, were described four years apart by Nel *et al.* (2004) and Perrichot *et al.* (2008), respectively. Perrichot *et al*. described the smaller-bodied †*G. occidentalis* as †*Sphecomyrmodes* in comparison to the type species of that genus – †*G. orientalis* from Kachin amber – without comparison to †*G. cretacica*. Unfortunately, given the current status of morphological knowledge, the holotypes of both †*G. orientalis* and †*G. cretacica* are too poorly preserved to allow for confident species-level identification. However, both Charentese species uniquely share a distinct, nearly squamiform petiolar shape, with the node being anteroposteriorly narrow and dorsoventrally tall; this indicates that the Charentese species are closely related to one another, relative to the Kachin species. For this reason, we group †*G. cretacica* and †*G. occidentalis* together in the *cretacica* species group. It is possible that †*G. cretacica* and †*G. occidentalis* are conspecific, but any taxonomic action should wait for the accumulation and processing of more material from the Charentese formation.

The identifiable Kachin species of †*Gerontoformica*, i.e. excluding †*G. orientalis*, †*G. rugosa* and †*G. tendir*, are evenly distributed in the *G. gracilis* and *G. pilosa* groups, with four species each. All species of the *pilosa* group are highly distinct in body form and setation, with †*G. sternorhabda* being an outlier, having the smallest body size and least pronounced constriction of the fourth abdominal segment, in addition to other defining features (see the species diagnosis below). In contrast, species of the newly recognized *gracilis* group are all largely similar to one another, without easily recognizable diagnostic structures. The most distinct Kachin species of the *gracilis* group is †*G. robusta*, which has a boxy mesosoma, with the meso- and metanota forming a nearly linear dorsal

margin in lateral view. The other species of the *gracilis* group have a multi-humped profile due to the bulge-like development of the meso- and metanota and are otherwise similar to one another (see Note 1 on the diagnosis of †*G. gracilis*).

†*GERONTOFORMICA STERNORHABDA* SP. NOV.

(FIGS 1C, D, 2C, F, I, L, 4–6, 7E, F, 11(1-2), 12(2-1, 2-3, 2-4), 13(3'-1); SUPPORTING INFORMATION, FIGS S1, S2)

Zoobank registration: urn:lsid:zoobank.org:act:E77C1A20-1398-465F-9607-AD11E97ADF1C

Type material: **Holotype**. Wingless female (w). Myanmar, Kachin State: Hukawng Valley [CASENT0741233 in an amber piece labelled AMNH SY-23 and deposited at AMNH]. **Paratypes**. Wingless females (w). Synincluded with holotype [CASENT0741234]; same locality as synincluded holo- and paratypes [UFV-LABECOL-009656, deposited in CELC].

Diagnosis (wingless female)

Conforming to the diagnosis of the Formicidae (see: Boudinot *et al*. 2020a, b), including the following key conditions: (1) postgenal bridge elongated, thus head 'prognathous' (Fig. 2C); (2) cranial condyles of the anterior/ dorsal mandibular articulation enlarged (Fig. 5B); (3) toruli oriented dorsolaterally rather than simply dorsally (Fig. 5A); (4) procoxae elongate, about twice as long as wide (Fig. 2C); (5) prodisticoxal foramen 'closed' and protrochanter narrowly necked (Fig. 4F) [Note 1]; (6) meso- and metathoracicocoxal articulations 'closed', i.e. directed ventrally rather than laterally or ventrolaterally (Fig. 4F); (7) abdominal segment II completely petiolated (Fig. 4F); (8) subpetiolar process present (Fig. 4F); (9) prora present (Fig. 4F).

I. **Among Formicidae, identifiable as †Sphecomyrminae:** (1) Mandibles simple and bidentate (Fig. 5A), without: (a) being strongly bowed and multidentate as in the †*Camelomecia* group, (b) the scythe-like blade as in the haidomyrmecine †*Haidomyrmex* clade, (c) projecting anteriorly with numerous teeth as in the haidomyrmecine †*Aquilomyrmex* clade, or (d) the strong torsion of †Zigrasimeciini (the state in †*Boltonimecia* is uncertain); (2) the antennal scrobes on the face do not extend all the way to the compound eye (Fig. 4B) (such scrobes observed in †Zigrasimeciinae, including †*Boltonimecia*) [Note 2]; (3) anterolateral corners of head not produced as robust triangles (Fig. 5A) (such corners observed in †*Dilobops* of the †Haidomyrmecinae); and (4) (a) scapes shorter than the width of the head (Fig. 5A) and (b) clypeus not extending posteriorly between the toruli (Fig. 2L) (such extension observed in †Brownimeciinae);

II. **Within †Sphecomyrminae, identifiable as †*Gerontoformica***: (5) anteromedian clypeal margin not produced as distinct medial lobe (Fig. 2L); vs. such a lobe present (†*Sphecomyrma*, †*G. tendir*) [Note 3]; and (6) (a) mandibles short and fitting against clypeus when closed (Fig. 5A) and (b) metanotum developed (Fig. 2C); vs. mandibles elongate and metanotum not developed (†*Myanmyrma*);

III. **Within †*Gerontoformica*, with the following unique condition**: (7) the anteroventral ('subpetiolar') process of the petiolar sternum long, orthogonal to the longitudinal axis of the petiole, and more-or-less rod-like, i.e. with anterior and posterior margins parallel to subparallel (Fig. 2C); vs. short and triangular (†*G. gracilis*, †*G. occidentalis*, †*G. pilosa*, †*G. robusta*, †*G. rugosa*, †*G. spiralis*, †*G. subcuspis*, †*G. tendir*) [Note 4];

IV. **Within †*Gerontoformica*, identifiable as a member of the *pilosa* species group**: (8) mesoscutum with distinct, raised transverse carina separating mesoscutal and mesoscutellar regions (Fig. 6B); vs. such a carina entirely absent or only poorly developed laterally, thus incomplete medially and not forming a distinct angle between the mesoscutal and mesoscutellar regions in profile view (*cretacica*, *gracilis* groups); (9) tergum of petiolar node anteroposteriorly longer than dorsoventrally tall (Fig. 2C); vs. petiolar node tergum taller than long (*cretacica* group); and (10) abdominal segment IV (metasomal III) with the cinctus distinct and impressed, i.e. divided into pre- and post-sclerites by a transverse sulcus (Fig. 5E);

V. **Within the *pilosa* species group, distinguished from all species by the following**: (11) cinctus developed, but transverse sulci weakly impressed, thus pre- and postsclerites of abdominal segment IV not meeting at strongly oblique angle (Fig. 5E); vs. transverse sulci deeply impressed, thus pre- and postsclerites meeting at distinct oblique angle (†*G. contega*, †*G. magna*, †*G. pilosa*); (12) head in full-face view broader laterally than long anteroposteriorly, excluding eyes (Fig. 2L); vs. head longer than broad (†*G. contega*, †*G. magna*, †*G. pilosa*) [Note 5]; (13) pretarsal claws edentate (Fig. 5G, I, J); vs. each claw with a single tooth of variable location (†*G. contega*, †*G. magna*, †*G. pilosa*) [Note 6]; and (14) body

small, mesosoma length < 1.5 mm (Fig. 2C); vs. body large, mesosoma length > 1.5 (†*G. contega*, †*G. pilosa*) and > 2.5 (†*G. magna*);

VI. Further distinguished by species in the *pilosa* group by the following: (15) anteromedian clypeal margin distinctly evenly curved to an 'incision' at the point of contact with the rounded lateroclypeal lobes (Fig. 2L); vs. anteromedian clypeal margin weakly convex, without distinct incision between the medioclypeus and lateroclypeal lobes, which are themselves anterolaterally angled (†*G. contega*); (16) in profile, pronotum evenly curved, mesoscutum more-or-less aligned with mesoscutellum and metanotum, and propodeal dorsal and posterior surfaces curving into one another obliquely (Fig. 2C); vs. pronotum, mesonotum, and propodeum each shouldered in appearance, i.e. pronotum with strong anterior dorsolateral bulge, mesonotum with mesoscutal and mesoscutellar regions meeting at nearly a right angle, and propodeal dorsal and posterior surfaces also meeting at nearly a right angle (†*G. contega*); (17) standing setation on body short, relatively sparse (with the exception of the propodeum and petiolar tergum) (Fig. 5); vs. longer setation present (†*G. magna*, †*G. pilosa*); and (18) anteroventral process of abdominal sternum III (metasomal II) robust but short anteroposteriorly (Fig. 2C); vs. prora anteroposteriorly long, shark-fin-like in form (†*G. pilosa*) [Note 7].

Notes on the diagnosis

Note 1: The right procoxa and protrochanter of the holotype are slightly disarticulated. However, the focal details to evaluate are the circular shape of the prodisticoxal foramen and the crank-like (curved) and thin proximal neck of the protrochanter, which can be evaluated from Figure 4F.

Note 2: The only species of †Sphecomyrminae to have an elongate antennal scrobe is †*G. contega*. Although the scrobe of this species was observed via direct examination of the holotype, it remains a possibility that this is an artefact because other specimens of †*Gerontoformica* may have asymmetrical, sulcus-like distortions of the head corresponding to the position of the scrobe (see the 'preservation' section of the †*G. gracilis* description; Fig. 10). Conducting a µ-CT scan of the type specimen and/ or the accrual of additional specimens are necessary.

Note 3: The anteromedian clypeal process of †*Sphecomyrma* is lateromedially thin and at least as long as broad; it is distinctly bordered laterally by the medioclypeus, i.e. the clypeal 'disc' between the lateral clypeal lobes. In contrast, the entire medioclypeus of †*G. tendir* is apparently produced. See Note 5 of the 'Notes on classification' section above.

Note 4: The form of the subpetiolar process is unknown for four species within the genus: †*G. contega*, †*G. cretacica*, †*G. magna* and †*G. orientalis*.

Note 5: Although it is difficult to evaluate the head shape of †*G. contega* from the holotype due to cut of the amber matrix, the head does appear to be longer than broad. Reevaluation of this condition through µ-CT is recommended.

Note 6: Teeth on the pretarsal claws have been recorded for most species of †*Gerontoformica* (†*G. contega*, †*G. gracilis*, †*G. magna*, †*G. occidentalis*, †*G. pilosa*, †*G. robusta*, †*G. spiralis* and †*G. subcuspis*). The condition of having reduced teeth on the pretarsal claws, however, is shared with †*G. cretacica* and †*G. tendir*. Notably, Perrichot *et al.* (2008) recorded minute teeth on the pretarsal claws of †*G. occidentalis*, which suggests the need to re-evaluate the holotype of †*G. cretacica*.

Note 7: The prora is clearly an important structural feature for distinguishing stem ants but is not clearly visible in most specimens, including †*G. contega* and †*G. magna* in the *pilosa* group, †*G. cretacica* and †*G. orientalis* in the *cretacica/orientalis* group, plus †*G. rugosa* and †*G. tendir*. It is extremely small and nearly absent in †*G. gracilis* and †*G. occidentalis*, and it is developed, but short and comparatively inconspicuous in †*G. robusta*, †*G. spiralis*, and †*G. subcuspis*.

Measurements and indices

Holotype, specimen C-33: HWed = 0.87; HWev = 0.95; EWl = 0.14; HD = 0.55; ML = 1.25; PnLi = 0.50; PnWa = 0.30; MnL = 0.27; AIIILm = 0.48; AIIILl = 0.53; HPI = 0.64; HSI = 0.69; AIIILI = 0.91.

Paratype, specimen C-34: HWed = 0.94; HWev = 1.06; EWl = 0.20; HD = 0.66; ML = 1.39; PnLi = 0.45; PnWa = 0.27; MnL = 0.28; AIIILm = 0.50; AIIILl = 0.64; HPI = 0.70; HSI = 0.67; AIIILI = 0.78.

UFV-LABECOL-009656: HWed = 0.79; HWev = 0.85; EWl = 0.11; HD = 0.46; ML = 1.05; PnLi = (~0.35–0.38); PnWa = –; MnL = 0.29; AIIILm = 0.4; AIIILl = 0.48; HPI = 0.58; HSI = 0.75; AIIILI = 0.83.

Description

Head: The **head** is broad in facial view, i.e. lateromedially wider than anteroposteriorly long from the anterior clypeal margin to the apparent posterior head margin (Fig. 2L); in posterior or lateral view, the head is dorsoventrally narrow, with the vertexal region not being particularly domed; standing setae are present on the vertexal and facial regions [Note 1]; there are short, decumbent setae distributed sparsely on the head capsule, a few longer, and suberect setae medially on the vertex near the ocelli. The **compound eyes** are situated in the posterior third of the head (Fig. 2L); they bulge laterally, breaking the silhouette of the lateral head margins in facial view; their height above the surrounding surfaces of the cranium is comparatively low; they comprise over 100 ommatidia, but not more than 200 (Fig. 4C) [Note 2]; they are apparently glabrous, i.e. lacking interstitial setation. The three **ocelli** are completely developed (Fig. 2L). The **frontal carinae** diverge posterolaterally, toward but not reaching the compound eyes (Figs 2L, 5A); they are sinuate in form, i.e. from their anterior margins they are directed relatively medially then bulge laterally before curving laterad; their anterior termini are close to the epistomal line, but not extending on to the clypeus; the minimum distance between the frontal carinae is about 0.29× maximum head width as measured in full face view. The **antennal scrobes**, or depressed contact surfaces of the face laterad the frontal carinae, are parallel in orientation relative to the frontal carinae and are apparently longer than wide (Figs 2L, 4B). The **antennal toruli** abut but do not indent the posterior clypeal margin [Note 3]; they are in the form of a low, more-or-less even ring. The **antennae** are 12-merous (Fig. 4B). The **scapes** are somewhat flattened and curved (Fig. 2C, F, I, L); they are about three to four times as long as wide (Fig. 2I); their length is about half the width of the head, and less than half the length of the head; they bear a vestiture of short subdecumbent to suberect setae. The **pedicels** are about twice as long as wide (Fig. 4F); they are about one-third the length of the scapes, and somewhat more than half the length of the third antennomere; their setation is similar to that of the scapes. The **flagellae** are longer than the mesosoma and are simple, i.e. not thickening distally (Fig. 4F); they bear a range of standing and appressed setae; **flagellomeres I** are the longest, being about four times as long as wide and more than half the length of the scapes; **flagellomeres II–IX** are about as long as the pedicel; **flagellomeres X** are longer than flagellomeres II–IX. The **clypeus** is about four times as wide (lateromedially) as long (anteroposteriorly), with the length measured from the midpoints of the anterior and posterior clypeal margins and the width measured between the lateralmost points of the clypeus (Fig. 2L). The **lateroclypeal areas** are formed as lateral lobes (Figs 2L, 5A). The **medioclypeal area** is anteriorly convex (Fig. 2L); its length at the midline of the head is about 0.21× head length also at midline, as measured in full-face view; it bears five or six long and flexuous setae that are situated near the anterior clypeal margin and anteriorly directed, consisting of one medial seta surrounded by a pair of setae and potentially a second, even more lateral pair [Note 4]; the anterior medioclypeal margin bears a row of chaetae. The **mandibles** are simple and apically bidentate (Fig. 5A). The **maxillary palps** are 5-merous (Figs 2I, 4A, 7E, F) [Notes 5, 6]; they are conspicuously short, with their total lengths shorter than the lengths of either the mandibles or scapes; with the exception of the apical palpomere, they are thick and bulging at about their midlengths; they are adorned with erect and appressed pilosity. The **labial palps** are 4-merous (Figs 2I, 4A, 7E, F) [Note 6]; they are short, being just over half the length of the maxillary palps; with the exception of the apical palpomere, they are more-or-less conical and thickening toward their apices; they are adorned with erect and appressed pilosity; the proximal palpomere lacks a distinct process.

Mesosoma: The **pronotum** bears an anteromedian neck process, and lateral and posteromedian flanges (Figs 2C, F, 5C, 6A); these flanges are flared in the paratype specimen C-34 (Fig. 4C) but not in the holotype or other paratype; the muscular node or 'disc' of the pronotum is almost spheroidal in shape, with the lateral margins strongly convex in dorsal view and the dorsal margin strongly convex in lateral view, and with an anteroposterior length approximating its dorsoventral height; pronotal setation is sparse, being represented by a few subdecumbent setae (Fig. 6A). The **pronotal lobes** are well developed (Fig. 6A) [Note 7]. The **mesonotum** is divided into an anterior mesoscutal area and a posterior mesoscutellar area by the **transverse mesonotal carina** (Figs 2C, F, 4C, F, 5C, 6B). The **mesoscutal area** is approximately in the form of a low saddle (i.e. is a low hyperbolic paraboloid), with a concave dorsal margin in lateral view, and with the anterior rim more upcurved than the posterior rim (Fig. 2C). The **mesoscutellar area** is convex, but sunken relative to the mesoscutal area (Fig. 2C). The **mesopectus** is divided into dorsal and ventral areas by a longitudinal sulcus (Fig. 2C); its dorsoventral height is about equal to its anteroposterior length. The **dorsal mesopectal area** is approximately rectangular in shape, being somewhat more than twice as long anteroposteriorly as tall dorsoventrally (Fig. 2C); its dorsoventral height is one-third the dorsoventral height of the lower mesopectal area as measured from

the transverse sulcus directly ventrad to an imaginary line drawn parallel to the ventrolateral margins of the meso- and metapecta. The **ventral mesopectal area** is approximately triangular in shape, being broad along is dorsal margin and narrowing posteroventrally to its ventrolateral margin (Fig. 2C); its anteroposterior length along its dorsal margin is approximately equal to its dorsoventral height. The **transverse mesometanotal sulcus** is anteroposteriorly short/ thin (Fig. 2C). The **metanotum** is developed as a distinct bulge between the metanotal spiracles (Fig. 2C). The **transverse metanotopropodeal sulcus** is anteroposteriorly long/ broad and continues ventrally toward the base of the mesocoxa, completely separating the lateral metapectal area from the lateral mesopectal area (Fig. 2C). The **metapleural gland orifice** is large, hairy, and in the form of a broad subelliptical pit (Fig. 6B); it is margined dorsally by a bulge, the **metapleural gland bulla**, and ventrally by the **ventral metapleural gland flange**, which itself is a continuation of the sinuate **ventrolateral carina of the metapectus** and is spiniform and dorsally inclined. The **propodeum** is boxy (Figs 2C, 6B) [Note 8]; it bears standing setae and is the hairiest mesosomal region. The **propodeal spiracles** are situated distant from the metanotum, but near the dorsal propodeal margin in lateral view (Figs 2C, 5C); they are posteriorly to posterolaterally directed and protected anteriorly by the **anterior flange of the propodeal** spiracles. The **propodeal lobes** are apparently not developed.

Legs: The legs are developed as expected for the Formicidae, with some notable characters and states. They are densely hairy, appearing shaggy, with the setae suberect (Fig. 4A, D, G–J). Apparently, the **apical protibial foramina** are open, i.e. without a bridge of sclerite dividing the calcar from the probasitarsus (Fig. 5G) [Note 9]. The **mesoprefemora** and **metaprefemora** are well developed and are broader ventrally than dorsally (Fig. 5D). The **protibia** bears and anterior brush of dense suberect setae in their apical third, near the calcar (Fig. 4A). Each of the **mesotibia** and **metatibia** bear a pair of apicoventral spurs (Figs 4I, H, 5H); the **anterior tibial spurs** are pectinate; the **posterior tibial spurs** are barbirulate to simple. The **calcar** is apparently bifid apically, with one point being the apex of the elongate **velum** and the other point a small array of hairs (Fig. 5G); two stout setae are developed (inserted) posterior to the calcar. The **plantar lobes** of the tarsi are not developed (absent), but the tarsomeres have a brush of dense ventral setae, and are apically margined by thick, coarse chaetae (Figs 4G–J, 5G–J) [Note 10]. The **fourth tarsomeres** of each leg are deeply notched distally, thus appearing V-shaped (probasitarsi) or arrowhead-shaped (meso-, metabasitarsi) (Fig. 4G–J). The **pretarsal claw teeth** are extremely small, only visible as weak bulges on the ventral margins of the claws (Fig. 5G, I, J). The **aroliae** of all legs are well-developed but comparatively small (Fig. 5G, I, J); they are ≤ 0.5× the length of the pretarsal claws.

Metasoma: The **petiole** is nodiform and lacks tergosternal fusion between its postsclerites (Figs 2C, 4F, 5F) [Note 11]. The **petiolar tergum** is anteriorly narrowed, has the spiracles situated on anterolateral bulges, and has a collar posterior to its node (Figs 2C, 5F); it bears several relatively long setae; setae on the remainder of the metasoma are gradually denser and longer from AIII–VII, with the greatest concentration around the sting. The **petiolar node** is anteroposteriorly longer than dorsoventrally tall (Fig. 2C, 5F); its anterior margin is longer than its posterior margin in lateral view, and these margins curve evenly into one another. The **laterotergites** are developed (present) (Fig. 5F), approximately wedge-shaped and broadening posteriorly. The **petiolar sternum** is anteriorly flat, with this region bearing stiff proprioceptor setae (Fig. 5F); its main portion is about twice as long anteroposteriorly as tall dorsoventrally (Figs 2C, 5F); it is broadly convex in cross-section at its midpoint (Fig. 2I); anteroventrally it is produced as the subdigitate to almost triangular **subpetiolar process**, which is at least twice as long dorsoventrally as wide anteroposteriorly (Figs 2C, 4F, 5F); posteriorly, the sternum is concave, appearing notched, with the concavity receiving the prora. The **helcium** (presclerites of the third abdominal segment) is narrow relative to the third abdominal postsclerites (Figs 2C, F, 4C, F) [Note 12]; the helcial tergite conceals the helcial sternite in lateral view (Fig. 5F). The **abdominal posttergite III** is somewhat constricted posteriorly and is not fused with the third abdominal poststernite (Fig. 2C); it is distinctly necked anteriorly, with a dorsoventrally short but distinct anterior surface which curves to the distinct 'node' of the sclerite; its 'node' is 'shouldered' in appearance, bulging anterolaterally around its 'neck', with the 'shoulders' visible over the ventrolateral tergal margins in ventral view (Fig. 2I) [Note 13]. The **abdominal tergosternal margin III** is weakly curved, without distinct 'shouldering' as observed in various Formicinae and Dolichoderinae (Fig. 2I) [Note 14]. The **abdominal poststernite III** is weakly constricted posteriorly, weakly angled lateromedially, and bears the prora anteroventrally (Fig. 2I). The **prora** is subdigitate in lateral view, being dorsoventrally long and anteroposteriorly thick (Fig. 2C); lateromedially, it is relatively narrow, and approximately wedge-shaped in ventral view

(Fig. 2I). The **abdominal segment IV** is neatly divided into pre- and post-sclerites by the **cinctus**, or transverse sulci on the tergum and sternum (Fig. 5E); its constriction is comparatively shallow. The **abdominal presclerites IV** are slightly narrower dorsoventrally and lateromedially relative to the postsclerites (Fig. 5E). The **abdominal poststernite IV** is shorter than the **abdominal posttergite IV**. The **abdominal segments V** and **VI** are undivided and are homonomous in form, i.e. highly similar in shape, size, and other qualities of appearance (Figs 2C, 4A, C, 5E). The **abdominal tergum VII** is approximately dome-shaped; *in situ*, its external surface is oriented dorsoventrally relative to the preceding segments (Fig. 5E). The **abdominal sternum VII** is lateromedially cupped and narrowed distally (Fig. 5E). The **sting** is long and narrow (Figs 4A, 5E). The **third valvulae** (sting sheaths) are digitate in form and exserted to highly exserted as preserved (Figs 4A, 5E) [Note 15].

Preservation: Both the holotype and the synincluded paratype (Fig. 4) have decomposition bubbles captured in the process of emanating from the head. The non-synincluded paratype (Fig. 5) has no such bubbles on the head, but some are present on the surface of the petiolar tergum, on some of the gastral tergites, and apparently a large one protrudes from the abdominal apex. The decomposition bubbles are associated with deformation of the cuticle, particularly for the holotype, where the affected cheek and fore tibia have bulged into the lumen of the bubble, as if displaced from compression. Three fracture lines are present around the head of the synincluded paratype, one approximately in the frontal plane, another at the base of the left antenna, and one between the head and pronotum. Finally, the metasoma of the synincluded paratype appears weakly desiccated (wrinkled); it is surrounded by a bubble that makes rendering difficult, but it is otherwise preserved well enough to determine fine details and structural proportions. Neither the holotype nor the non-synincluded paratype have fracture lines or apparent desiccation.

Notes on the description

Note 1: The setation of the body, in general, could not be described in fine detail.

Note 2: The ommatidia were counted for one eye of the paratype from a high-resolution photograph. It was not possible to count all of the ommatidia for this eye. Likewise, we counted 85 ommatidia in the left eye of the non-synincluded paratype; about 15% of this eye is concealed, so we expect that there are indeed > 100 ommatidia, but certainly less than 150.

Note 3: The position of the antennal toruli relative to the posterior clypeal margin is known to be of classificatory value above the species level (Bolton, 2003). We observe that the toruli contact the epistomal line in †*G. sternorhabda,* but do not provide this in the diagnosis because the posterior limit of the clypeus is difficult to evaluate in some of the fossils, particularly in the type specimens of the *gracilis* group. However, among the *pilosa* group, we observed that the toruli are close to or abutting the clypeus in †*G. contega* and †*G. pilosa*. It is difficult to determine the posterior extent of the clypeus in †*G. magna*, thus no confident statement can be made at this time.

Note 4: The setae on the medioclypeal area could only be evaluated on the non-synincluded paratype. The lateralmost seta is probably paired, but the second hair could not be observed.

Note 5: We have recorded the maxillary palps as 5-merous based on scrutiny of the non-synincluded paratype (Fig. 5B, C) and our renders of the synincluded types (Fig. 7E, F). It is possible that there is a poorly developed proximal sixth palpomere ('pm?' in Fig. 7E, F). The palps are remarkably short compared to those of †*G. gracilis*, and they lack the process of the proximal labial palpomere which we observed in the other species.

Note 6: The shape of the palpomeres is notable, as the proximal ones appear flattened to some degree. Extended µ-CT sampling is recommended to understand palpomere shape variation.

Note 7: The pronotal lobes of †*Gerontoformica* are large compared to crown ants. Systematic evaluation of the development of these lobes among stem ants is recommended.

Note 8: The shape of the propodeum appears to differ between the two synincluded types and the non-synincluded type. While the propodeum is rounded in the non-synincluded specimen, it is somewhat rectangular in the synincluded specimens, with the dorsal and posterior margins oriented nearly perpendicularly and narrowly rounding into one another in lateral view, and its posterior surface nearly flat.

Note 9: We have stated 'apparently', as we are not totally certain about this state. We have included it, however, in order to encourage future examination of this structure, which we know to be variable across the Formicidae and other groups of Aculeata (B. E. B., pers. obs.).

Note 10: Plantar lobes are developed in †*G. gracilis*, which has far sparser ventral tarsomeral setae and proportionally larger aroliae. Because tarsal setae, lobes and aroliae are functional traits related to traction (e.g. Beutel & Gorb 2001; Boudinot *et al.* 2021a; Wöhrl *et al.* 2021), the distinctions observed here suggest, or otherwise indicate, that there is niche separation between †*G. sternorhabda* and †*G. gracilis*. Among *pilosa* group species, the fourth tarsomeres are notched in †*G. contega*, are *gracilis*-like in †*G. pilosa*, and are of uncertain form in †*G. magna*.

Note 11: Whereas it was possible to determine whether or not the postsclerites of the metasoma were fused, it was not possible to evaluate such fusion for the presclerites of the petiole and third abdominal segment.

Note 12: The helcium of †*G. sternorhabda* is distinctly broader than that of †*G. gracilis*. However, it was not possible to evaluate this condition for the other previously described †*Gerontoformica* species.

Note 13: Abdominal tergum III of the non-synincluded paratype is apparently not similarly shouldered. We are, therefore, less certain about the development and distribution of this state, i.e. whether it is artefactual or not, or whether the additional paratype is indeed conspecific. We choose to recognize the additional paratype as conspecific due to the high degree of shared conditions, as indicated by the diagnosis. We also consider the tergal shouldering to likely be a true developmental state of †*G. sternorhabda*, as we observe it in both of the synincluded specimens, and as the synincluded †*G. gracilis* clearly does not display this condition. The third abdominal postsclerite is more-or-less evenly curved from anterior to posterior (†*G. pilosa*) or is entirely evenly curved from anterior to posterior (†*G. gracilis*, †*G. robusta*, †*G. spiralis* and †*G. subcuspis*); it could not be confidently determined for †*G. occidentalis* or for the four *nomina dubia* species.

Note 14: Shouldering of the third abdominal tergosternal margin was used for generic identification and the tribe-level classifications of the Formicinae and Dolichoderinae by Bolton (1994, 2003). We perceive no difference in the form of these margins between †*G. sternorhabda* and †*G. gracilis*; we encourage evaluation of the form of the margins for other stem Formicidae.

Note 15: We anticipate that study of the sting apparati of stem ants using μ-CT to be fruitful. The degree to which the third valvulae are exserted is unusual.

Remarks on the description

The non-synincluded paratype (UFV-LABECOL-009656) may not be conspecific with the synincluded type specimens. It differs from the synincluded specimens by the following states: (1) possibly in maxillary palpomere count (5 vs. 6; see Note 5 of the description); (2) the propodeal spiracle appears to be slightly higher on the propodeum; (3) the propodeum appears to be more rounded; (4) the petiolar node appears to be shorter; (5) the subpetiolar process appears to be straighter; and (6) the third abdominal posttergite does not appear to be shouldered. We note that these are 'apparent' differences because of the limited set of available specimens. Based on expectations from the neontological fauna, it is possible that the differences we observe may be infraspecific variation, but it will be necessary to evaluate more specimens. Because the specimens from the two pieces of amber are otherwise highly similar and equally diagnosable, we conservatively designate them as conspecific.

Etymology

The specific epithet *sternorhabda* combines the Ancient Greek words στερνών (sternum) and ράβδος (rod) in reference to the form of the subpetiolar process, which is unique among †*Gerontoformica*. The name is adjectival and feminine in form to match the gender of the genus.

†*GERONTOFORMICA GRACILIS* (BARDEN & GRIMALDI, 2014)

(FIGS 1A, B, 2A, B, D, E, G, H, J, K, 8, 9, 10, 11(1'-2), 12(7-1); SUPPORTING INFORMATION, FIG. S3)

†*Sphecomyrmodes gracilis* Barden & Grimaldi, 2014: 4–7, figs 2, 10B, 11C, D (wingless female, Kachin amber, JZC-Bu324A, AMNH).
Combination in †*Gerontoformica*: Barden & Grimaldi (2016): 518, suppl. info. p. 16.

Diagnosis (wingless female)

Similarly identifiable as †*G. sternorhabda* to the genus †*Gerontoformica* (I–III above), including absence of the anteromedian lobate clypeal process [Note 1]. For the diagnosis and redescription, see Figures 2, 8 and 10 primarily.

I. **Among †*Gerontoformica*, with the following unique character**: (1) proximal labial palpomere with a distinct, apicomedially situated lobate process (Fig. 7A, B) [Note 2];
II. **Within †*Gerontoformica*, identifiable as a member of the *gracilis* species group**: (2)

Figure 4. Photomicrographs of †*G. sternorhabda* sp. nov. showing setation and certain key features. A–D, G–I, paratype, CASENT0741234. E, F, J, holotype, CASENT0741233. A, body, ventrolateral oblique view. B, head, dorsolateral oblique view. C–F, body and left legs: D, dorsolateral oblique; (F) is slightly offset from (E), revealing the prora and subpetiolar process. G, protarsus, posterodorsal oblique view. H, mesotarsus, dorsal view. I, metatarsus, dorsal view. J, metatarsus, posterior view. Abbreviations: ad, antennomere distorted, i.e. visibly distorted antennomere associated with decay bubble; cn, cinctus; ms, metanotal spiracle; pr, prora; psf, anterior flange of propodeal spiracle; ptb, probasitarsal brush; spp, subpetiolar process; ss, standing setae; tnc, transverse mesonotal carina.

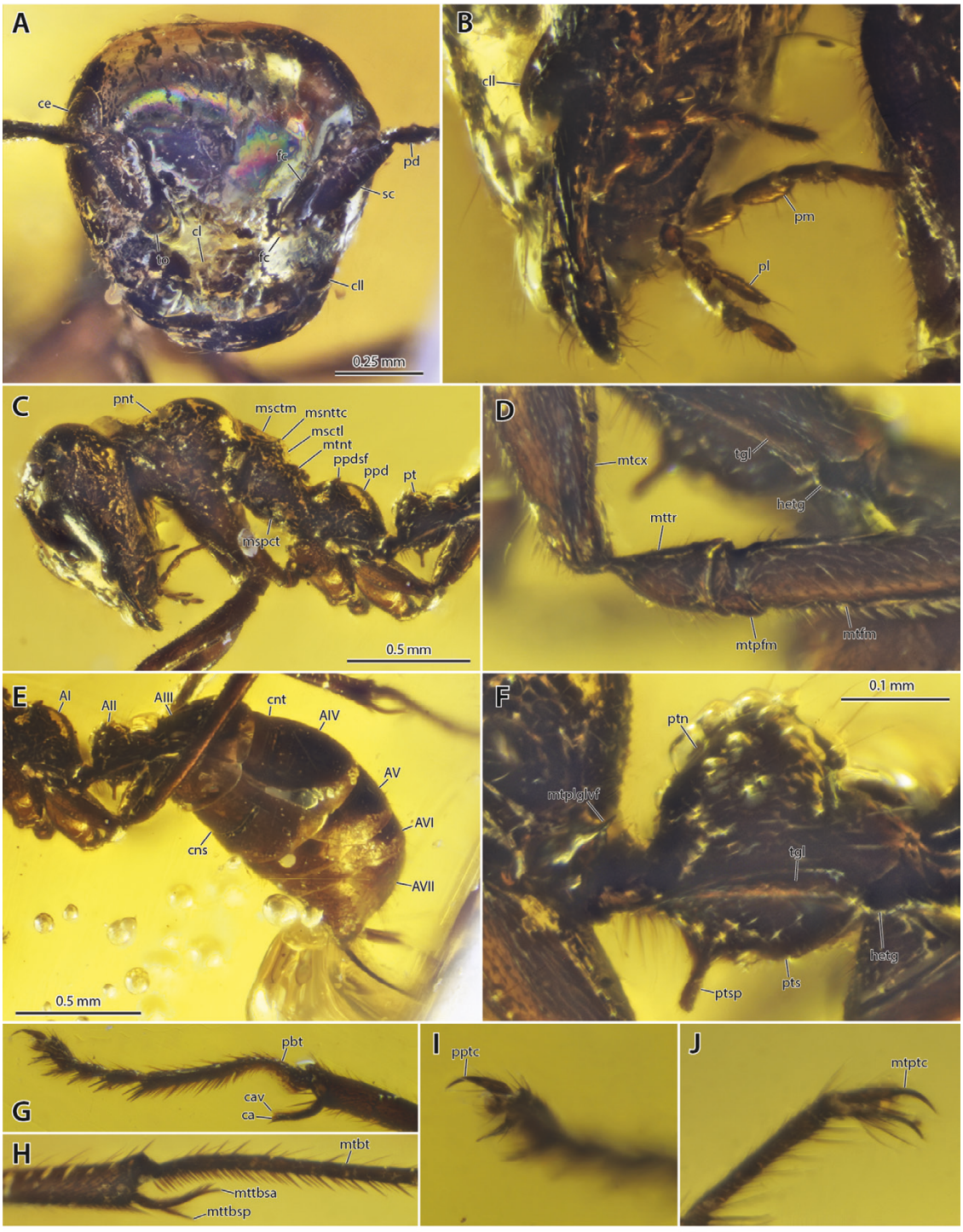

Figure 5. Photomicrographic details of †*G. sternorhabda* sp. nov. Paratype specimen (UFV-LABECOL-009656). A, head in approximate facial view. B, mouthparts in anterolateral oblique view. C, head and mesosoma in lateral view. D, proximal segments of metathoracic leg in approximate anterior view. E, metasoma in approximate lateral view. F, petiole in lateral view. G, prothoracic tarsus, oblique posterior view. H, metatibial apex and metabasitarsal base in posterior view. I, propretarsus in oblique distal view. J, metapretarsus in posteroventral oblique view. Abbreviations: AI, propodeum; AII–AVII, second through seventh abdominal segments; ca, calcar; cav, velum (lamella) of calcar; ce, compound eye; cl, clypeus; cll, lateral lobe of clypeus; cns, cinctus of fourth abdominal sternum; cnt, cinctus of fourth abdominal tergum; fc, frontal carina; hetg, helcial tergite; msctl, mesoscutellar area (mesoscutellum); msctm, mesoscutal area (mesoscutum); msnttc, transverse

mesoscutum without distinct, raised transverse carina separating mesoscutal and mesoscutellar regions (Fig. 10A); (3) tergum of petiolar node anteroposteriorly longer than dorsoventrally tall (high); and (4) abdominal segment IV without cinctus dividing the tergum and sternum into pre- and postsclerites;

III. **Within the *gracilis* species group, identified by the following**: (5) petiole bun-like, with anteroposteriorly long node; vs. subsquamiform, with anteroposteriorly narrow node (†*G. cretacica* and †*G. occidentalis*); (6) meso- and metanota bulging, with their dorsal silhouette bihumped; vs. meso- and metanota not bulging, with their dorsal silhouette forming an almost straight line (†*G. robusta*); (7) transverse dorsal sulci of mesosoma broad, separating the meso- and metanota and the metanotum and propodeum by at least one tarsomere width; vs. these sulci not as broad, with the meso- and metanota and the metanotum and propodeum separated by less than one tarsomeral width (†*G. spiralis*, †*G. subcuspis*) [Note 1]; and (8) propodeal spiracle covered anteriorly by an anterior flange which is directed posterolaterally; vs. spiracle not flanged (†*G. spiralis*, †*G. subcuspis*; state uncertain for †*G. robusta*) [Note 3].

Notes on the diagnosis

Note 1: †*Gerontoformica gracilis* is quite similar overall to †*G. spiralis* and †*G. subcuspis*. The primary structural distinction is the width of the dorsal transverse sulci that divide the mesonotal and metanotal regions, and the metanotal region and the propodeum, as well as development of an anterior flange around the propodeal spiracles. The character used by Barden & Grimaldi (2014) to distinguish †*G. spiralis* and †*G. gracilis* was the distance between the pro- and mesocoxae (their couplet 9); this is certainly a matter of preservation, as the prothorax of the holotype of †*G. gracilis* is elevated relative to the mesothorax, and the coxae are promoted anteriorly. Such pronotal elevation is possible in ant species with a mobile promesonotal articulation. The defining feature of †*G. subcuspis* provided by Barden & Grimaldi (2014) is the form of the subpetiolar process, which has an almost vertically oriented anterior margin in profile view. The process of †*G. gracilis* is more evenly rounded from posterior to anterior, while that of †*G. spiralis* is not visible. These distinctions should be re-evaluated in future study. See also Note 3 on the synopsis of †*Gerontoformica* classification above.

Note 2: We do not know the distribution of the process of the proximal labial palpomere across †*Gerontoformica*, with the exception of its absence in †*G. sternorhabda*. Despite this, we note the development of these processes as they are unique to our knowledge of both extant and extinct species. Because of the difficulty of evaluating proximal palpomeres for ants in general, and especially for fossil ants, we strongly recommend the application of µ-CT methods to determine the phylogenetic extent of this obvious apomorphy. Note that it is possible that the holotype lacks this condition, as we discovered this character after our chance to directly examine the type specimen.

Note 3: The anterior flange or hood of the propodeal spiracle is present in most †*Gerontoformica* examined, with the exception of †*G. spiralis* and †*G. subcuspis*. The flange could not be evaluated for †*G. magna* or †*G. robusta*.

Measurements and indices

Adult, specimen C-32: HWed = 0.71; HWev = 0.78; EWl = 0.17; HD = 0.62; ML = 1.49; PnLi = 0.59; PnWa = 0.18; MnL = 0.35; AIIILm = 0.52; AIIILl = 0.65; HPI = 0.99; HSI = 0.47; AIIILI = 0.80.

Pupa, specimen C-31: HWed = 0.72; HWev = 0.71; EWl = 0.18; HD = 0.62; ML = 1.62; PnLi = 0.60; PnWa = 0.25; MnL = 0.34; AIIILm = 0.62; AIIILl = 0.73; HPI = 0.86; HSI = 0.44; AIIILI = 0.85.

Redescription: adult

Head: The **head** is narrow in facial view, i.e. it is lateromedially narrower than anteroposteriorly long as measured from the anterior clypeal margin to the apparent posterior head margin (Fig. 2K); in posterior and lateral view, the head is dorsoventrally broad, with the vertexal region dome-like; standing setae are most conspicuous on the clypeus. The **compound eyes** are situated in the posterior third of the head; they bulge laterally, breaking the silhouette of the lateral head margins in facial view; their height

mesonotal carina; mspct, mesopectus; mtbt, metabasitarsus; mtcx, metacoxa; mtfm, metafemur; mtnt, metanotum; mtpfm, metaprefemur; mtplglvf, ventral flange of the metapleural gland; mtptc, metapretarsal claw; mttbsa, anterior spur of metatibia; mttbsp, posterior spur of metatibia; mttr, metatrochanter; pd, pedicel; pl, labial palp; pm, maxillary palp; pbt, probasitarsus; pnt, pronotum; ppd, propodeum; ppdsf, anterior flange of propodeal spiracle; pptc, propretarsal claw; pt, petiole; ptn, petiolar node; pts, petiolar sternum; ptsp, subpetiolar process; sc, scape; tgl, laterotergite; to, antennal torulus.

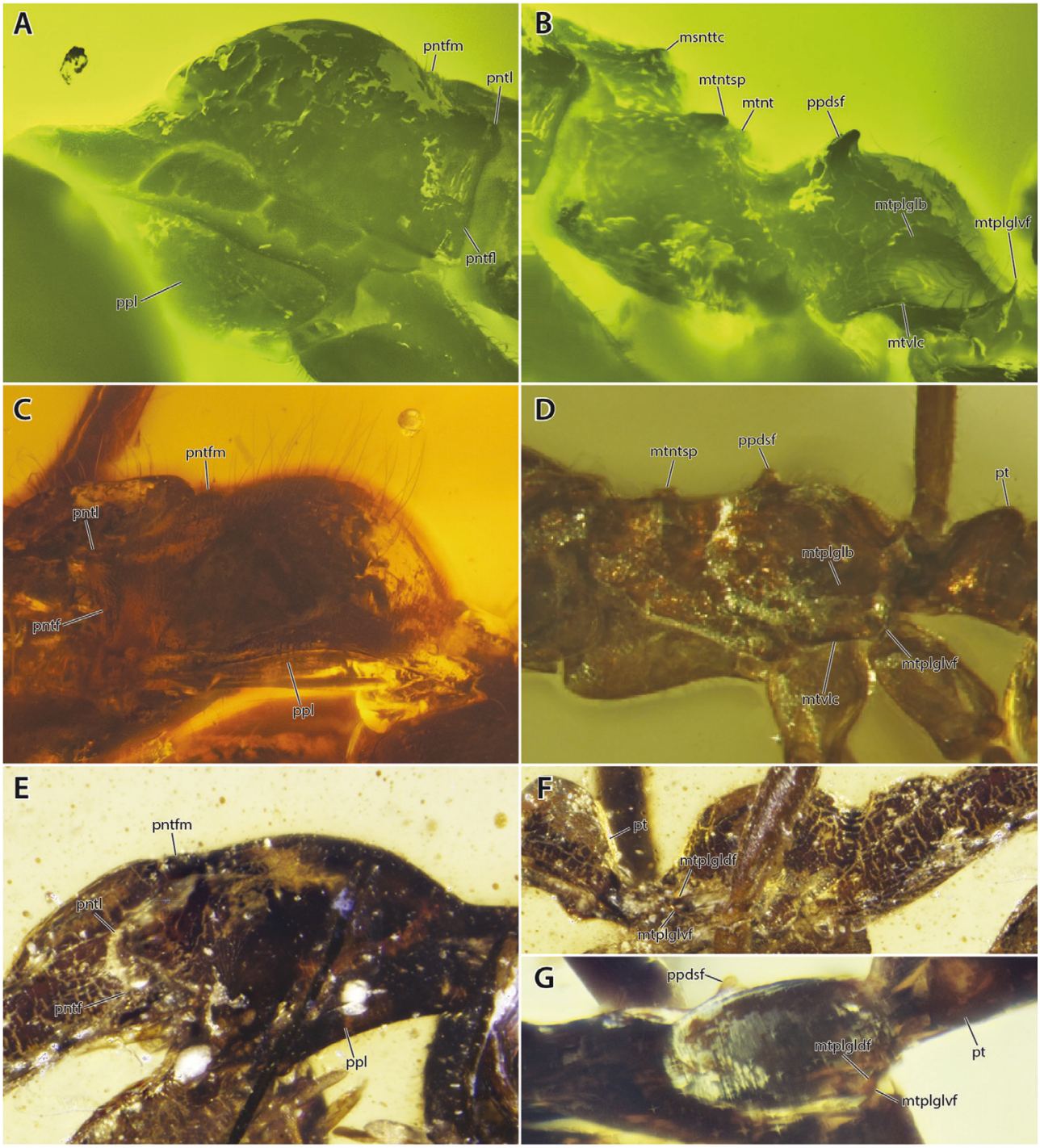

Figure 6. Details of the pronota and metapleural glands of †*Gerontoformica*. A, B, fluorescent light microscopy; C–G, standard photomicroscopy. A, B, †*G. sternorhabda* sp. nov. paratype (UFV-LABECOL-009656). C, †*G. pilosa* (ANTWEB1038931). D, †*G. sternorhabda* sp. nov. non-type (JWJ-BU21). E, F, †*G. gracilis* holotype (JZC-Bu324A). G, †*G.* near or conspecific with *gracilis* (ANTWEB1032649). Abbreviations: msnttc, transverse carina of mesonotum; mtplglb, metapleural gland bulla; mtplgldf, metapleural gland dorsal flange; mtplglvf, metapleural gland ventral flange; mtvlc, ventrolateral carina of metathorax; mtntsp, metanotal spiracle; mtnt, metanotum; pntl, pronotal lobe; pntfl, lateral pronotal flange; pntfm, medial pronotal flange; ppdsf, anterior flange of propodeal spiracle; ppl, propleuron; pt, petiole.

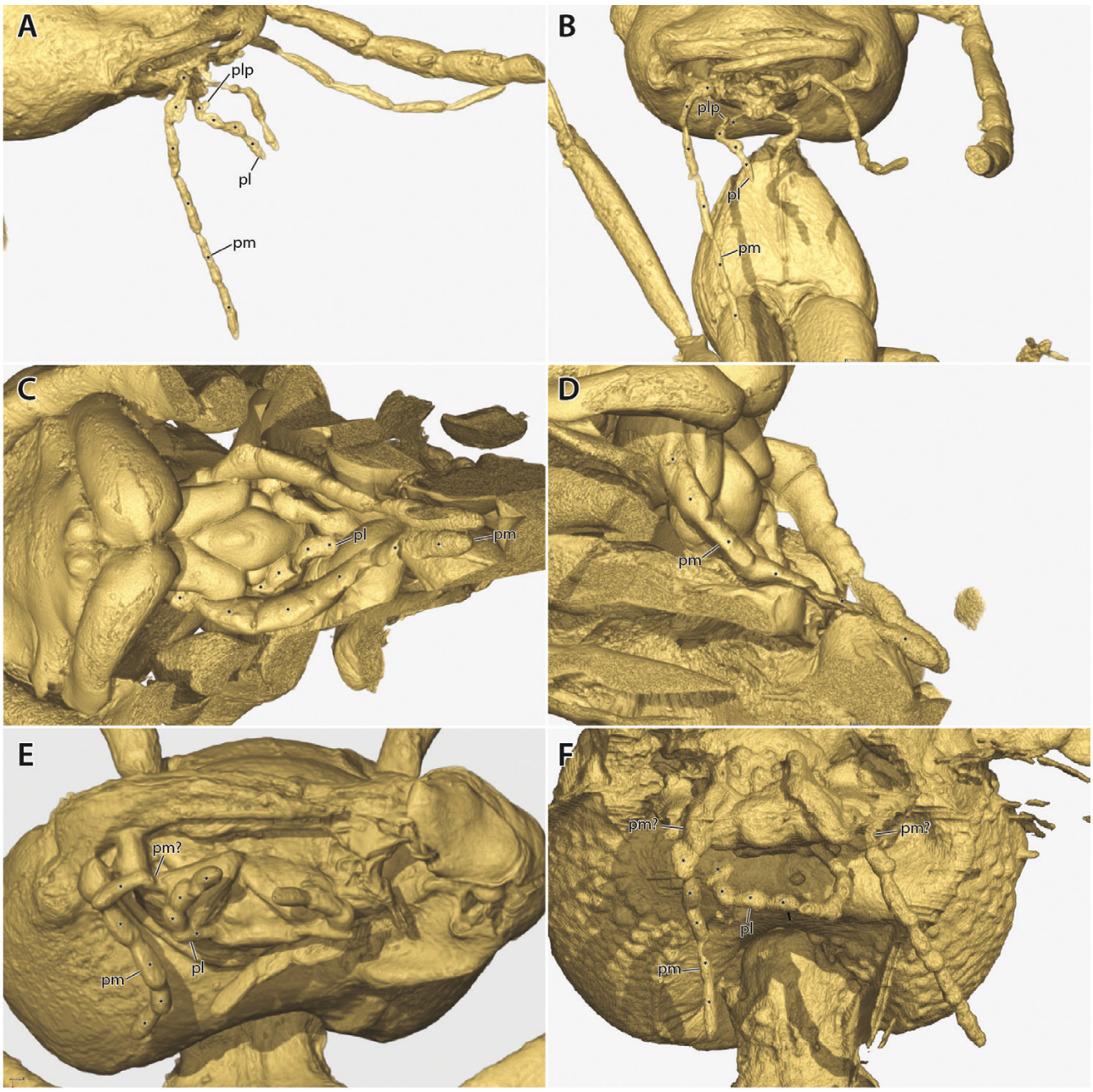

Figure 7. Maxillary and labial palps of †*G. gracilis* and †*G. sternorhabda* sp. nov.. Small black stars indicate each palpomere on the right-hand side of the body. A, B, †*G. gracilis* adult, CASENT0741232, in anterior dorsolateral oblique view (A) and anterior view (B). C, D, †*G. gracilis* pupa, CASENT0741231, in anterior view (C) and anterior dorsolateral view (D). E, F, †*G. sternorhabda* sp. nov. holotype, CASENT0741233, and paratype, CASENT0741234, in anteroventral oblique view. Abbreviations: pl, labial palp; plp, process of the proximal labial palpomere; pm, maxillary palp; pm?, possible maxillary palpomere.

above the surrounding surfaces of the cranium is comparatively high; their ommatidia count appears similar to that of †*G. sternorhabda*; they are apparently glabrous, i.e. lacking interstitial setation. The three **ocelli** are completely developed. The **frontal carinae** diverge posterolaterally toward but not reaching the compound eyes; they are circular in form, i.e. curving evenly from their anterior termini to their posterior termini which are directed anterolaterally, rather than posterolaterally; their anterior termini are distant from the epistomal line; the minimum distance between the frontal carinae is about 0.26× maximum head width

as measured in full face view. The **antennal scrobes** are anteroposteriorly short and encircled by the frontal carina. The **antennal toruli** are distant from the posterior clypeal margin; they are in the form of a low, more-or-less even ring. The **antennae** are 12-merous. The **scapes** are somewhat flattened and curved; they are about four times as long as their maximum width; their length is somewhat more than half the width of the head, and somewhat less than half the length of the head; they lack standing setae along their shafts. The **pedicels** are slightly longer than twice their width; they are about one-third the length of the scapes, and about half the length of the third antennomere; they apparently lack standing setae. The **flagellae** are longer than the mesosoma and are simple, i.e. not thickening distally; they bear a range of standing and appressed setae; **flagellomeres I** are the longest, being somewhat more than four times as long as wide and about three fourths the length of the scape; **flagellomeres II–IX** are all longer than the pedicel; **flagellomeres X** are longer than each pair of flagellomeres from II to IX. The **clypeus** is about three times as wide lateromedially as long anteroposteriorly, with the length measured from the midpoints of the anterior and posterior clypeal margins and the width measured between the lateralmost points of the clypeus. The **lateroclypeal areas** are formed as lateral lobes. The **medioclypeal area** is anteriorly convex; its length at the midline of the head is about 0.21× head length also at midline, as measured in full-face view; it bears an array of standing (rather than appressed) setae on its disc and is margined anteriorly by chaetae. The **mandibles** are simple and apically bidentate. The **maxillary palps** are 6-merous (Figs 2B, H, 7A–D) [Note 1]; they are elongate, being almost as long as the head and longer than the scapes and mandibles; the proximal palpomeres are short compared to the others; the second palpomeres are dorsoventrally flattened and lobate apicomedially; the third through sixth palpomeres are long, thin, and cylindrical. The **labial palps** are 4-merous (Figs 2B, H, 7A–D) [Note 1]; they are short, being less than half the length of the maxillary palps, and with their individual lengths shorter than each of the maxillary palpomeres with the exception of the proximal maxillary ones; the proximal labial palpomere is narrow proximally and bears a distinct lobate process medially at about its apical third, with this process being about as long as wide; the second and third palpomeres are thickened medially; the fourth palpomeres are relatively more cylindrical.

Mesosoma: The **pronotum** bears an anteromedian neck process, and lateral and posteromedian flanges; these flanges are not flared; the muscular node or 'disc' of the pronotum is hemispherical as observed in lateral view and almost elliptical in dorsal view, being distinctly longer than tall in lateral (profile) view, thus appearing narrow; setation was not observed on the pronotum [Note 2]. The **pronotal lobes** are well developed (Fig. 6E). The **mesonotum** is not divided into an anterior mesoscutal area and a posterior mesoscutellar area, i.e. the **transverse mesonotal carina** is not developed; the notum is convex in lateral view and is almost flattened along most of its length. The **mesopectus** is not clearly divided into dorsal and ventral areas; its dorsoventral height is almost 1.5× that of its anteroposterior length. The **transverse mesonotal sulcus** is anteroposteriorly long/broad. The **metanotum** is developed as a distinct and almost evenly convex bulge. The **transverse metanotopropodeal sulcus** is anteroposteriorly broad and continues ventrally toward the base of the mesocoxa, completely separating the lateral metapectal area from the lateral mesopectal area. The **metapleural gland orifice** is small and not remarkably hairy (Fig. 6F); it does not have a distinct bulla; it is margined dorsally and ventrally by flanges, including the **ventral metapleural gland flange**. The **propodeum** is rounded, with the dorsal and posterior margins curving broadly into one another in lateral view; its posterior surface is convex; it does not, apparently, bear standing setae. The **propodeal spiracles** are situated distant from the metanotum and below the dorsal propodeal margin as seen in lateral view, but they are located in the anterodorsal fourth of the sclerite. The **propodeal lobes** are apparently not developed.

Legs: The legs are developed as expected for the Formicidae, with some notable characters and states. With the exception of the tibial apex and tarsi, they appear almost entirely glabrous. The state of the **apical protibial foramina** is uncertain. The **mesoprefemora** and **metaprefemora** are well-developed and are broader ventrally than dorsally. The **protibia** bears and anterior brush of dense suberect setae in their apical third, near the calcar. Each of the **mesotibia** and **metatibia** bear a pair of apicoventral spurs; the **anterior tibial spurs** are barbirulate; the **posterior tibial spurs** are simple. The **calcar** is apparently bifid apically, with one point being the apex of the elongate **velum** and the other point being a small array of hairs; two stout setae are developed posterior to the calcar. The **plantar lobes** of the tarsi are well developed, the ventral setation is sparse, and the apical row of chaetae is thinner. The **fourth tarsomeres** are only weakly notched distally, thus appearing cylindrical in dorsal view. The **pretarsal claw teeth** are well developed and located just past the midlength of their respective claws. The **aroliae** are well developed and comparatively large (Fig. 8D); they are nearly as long as the pretarsal claws.

Metasoma: The **petiole** is nodiform and lacks tergosternal fusion between its postsclerites. The **petiolar tergum** is anteroposteriorly longer than dorsoventrally tall; it is asymmetrically convex, being somewhat longer anteriorly than posteriorly. The developmental state of the **laterotergites** is uncertain. The **petiolar sternum** is anteriorly flat; its main portion is at least twice as long as tall; it is narrowly convex in cross-section at its midpoint; it is weakly produced anteroventrally as a low, lobate **subpetiolar process**, which is shorter dorsoventrally than wide anteroposteriorly; posteriorly, the sternum is not distinctly concave or notched. The **helcium** is narrow relative to the third abdominal postsclerites; the helcial tergite conceals the helcial sternite in lateral view. The **abdominal posttergite III** is not constricted posteriorly and is not fused with the third poststernite; it is not necked or shouldered anteriorly, as the tergum evenly curves from its anterior base to posterior margin in lateral view. The **abdominal tergosternal margin III** is weakly curved, without distinct 'shouldering' as observed in various Formicinae and Dolichoderinae. The **abdominal poststernite III** is not constricted posteriorly, but is weakly angled lateromedially, and bears the prora anteroventrally. The **prora** is lip-like in lateral view, being anteroposteriorly short and more-or-less transverse in ventral view. The **abdominal segments IV**, **V**, and **VI** are not divided into pre- and postsclerites by a cinctus; they are homonomous in form, i.e. highly similar in shape, size and other qualities of appearance. The **seventh abdominal tergum** is somewhat dome-like. The **seventh abdominal sternum** is lateromedially cupped and narrowed distally. The **sting** is long and narrow. The **third valvulae** are digitate in form and highly exserted as preserved.

Preservation: The specimen CASENT0741232 is exceptionally well preserved internally, particularly the head and mesosoma (Fig. 9). The metasoma is, however, less well preserved, and has some apparent fungal growth or decay bubbling emanating from between the third and fourth abdominal segments. There are several fractures around the specimen, including on the dorsal surface of the head, the ventral right side of the head, across the left side of the mesosoma, and across the petiole and the left side of the third and fourth abdominal segments. The right side of the face, opposite from where the scape is held, is indented, thus appearing to have a longitudinal scrobe (Fig. 10); this is definitely an artefact, as it is not symmetrically present on the left side of the face where the scape is preserved in a position that is distant from the head capsule. Similarly, the mesosoma is indented where the legs are in close proximity (Fig. 10). The left metatrochanter appears distorted in shape.

Notes on description

Note 1: The original description recognized 4-merous maxillary palps and did not state a labial palpomere count. A 6, 4 palp formula (*sensu* Bolton, 1994, 2003) was determined here based on direct examination of the holotype, and from our microphotographs and digital renders. As noted in the diagnosis, the process of the proximal labial palpomere is unique among †*Gerontoformica*, given our current knowledge.

Note 2: We are not certain whether †*G. gracilis* is largely glabrous or whether it has appressed pubescence in various places. At the least we expect pubescence on inter-sclerite contact surfaces.

Description: pupa

The pupa (Figs 2A, D, G, J, 7, 10) is encased in a cocoon with a black meconium at the caudal end (Fig. 1A). Most structures of species-level identificatory value are incompletely developed, including the frontal carinae, perioral sclerites, mesosomal dorsum and anterior metasoma. The preservation of the specimen is fine externally but is poor internally, with the body cavity filled with a single, solid mass, despite apparent distinctions as seen from light microscopy. In overall appearance, the specimen is relatively bubbly or puffy looking, and has the propodeum crushed and incompletely differentiated from the petiole. Those metasomal segments which are posterior to the petiole are bulging, thus they appear slightly constricted as with a cinctus, but cincti are apparently absent. The metanotal and propodeal spiracles are visible externally, but those of the metasoma are not.

Features of note include the following: The head is longer anteroposteriorly than broad lateromedially; the mandibles are contacting one another apically; the maxillolabial complex is exserted, with the palps and glossa clearly visible in ventral view; the maxillary palps are 6-merous; the labial palps are 4-merous; the antennae are directed caudally and reach the posterior margin of the third abdominal segment; the pronotum is longer than tall in lateral view; and the mesonotum lacks a transverse ridge, thus is not divided into anterior mesoscutal and posterior mesoscutellar regions.

The pupa differs from the synincluded adults of both species as follows: The antennae appear wideset; the clypeus is anteroposteriorly longer, apparently with an additional band of cuticle along the anterior margin; the mandibles are obliquely oriented relative to head length, converging anterad (vs. perpendicular to the long axis of the head at closure); and the labrum is apically notched and with distinct paramedian lobes.

Remarks on the pupa

Because little comparative work on pupal morphology has been done in Formicidae, it is basically unknown what the polarity of the 'general features of note' is within the family. Further, because there are no developmental series of anatomy available for pupal transformation, we cannot be certain of the stage that this specimen was preserved. The conditions listed above which differ between the pupa and adults are especially interesting, as they suggest that there are intermediate stages in the structural rearrangement of the body. For example, the wideset toruli and exceptionally long clypeus are hard to explain without an atlas of developmental transformation. We note the apically bilobate labrum, in particular, as the labra of the adults are apically rounded. At present we are unable to explain the labral difference, as there are no works that model the developmental transformation from immature to imago in ants; such studies are much needed (for further detail, see: Boudinot *et al.*, 2021b).

DISCUSSION

Here we report the discovery of a Mid-Cretaceous Kachin amber fossil which contains three wingless adult females and a wingless pupal female of the stem ant genus †*Gerontoformica* (Fig. 1). This is the first record of the syninclusion of multiple life stages of Mesozoic

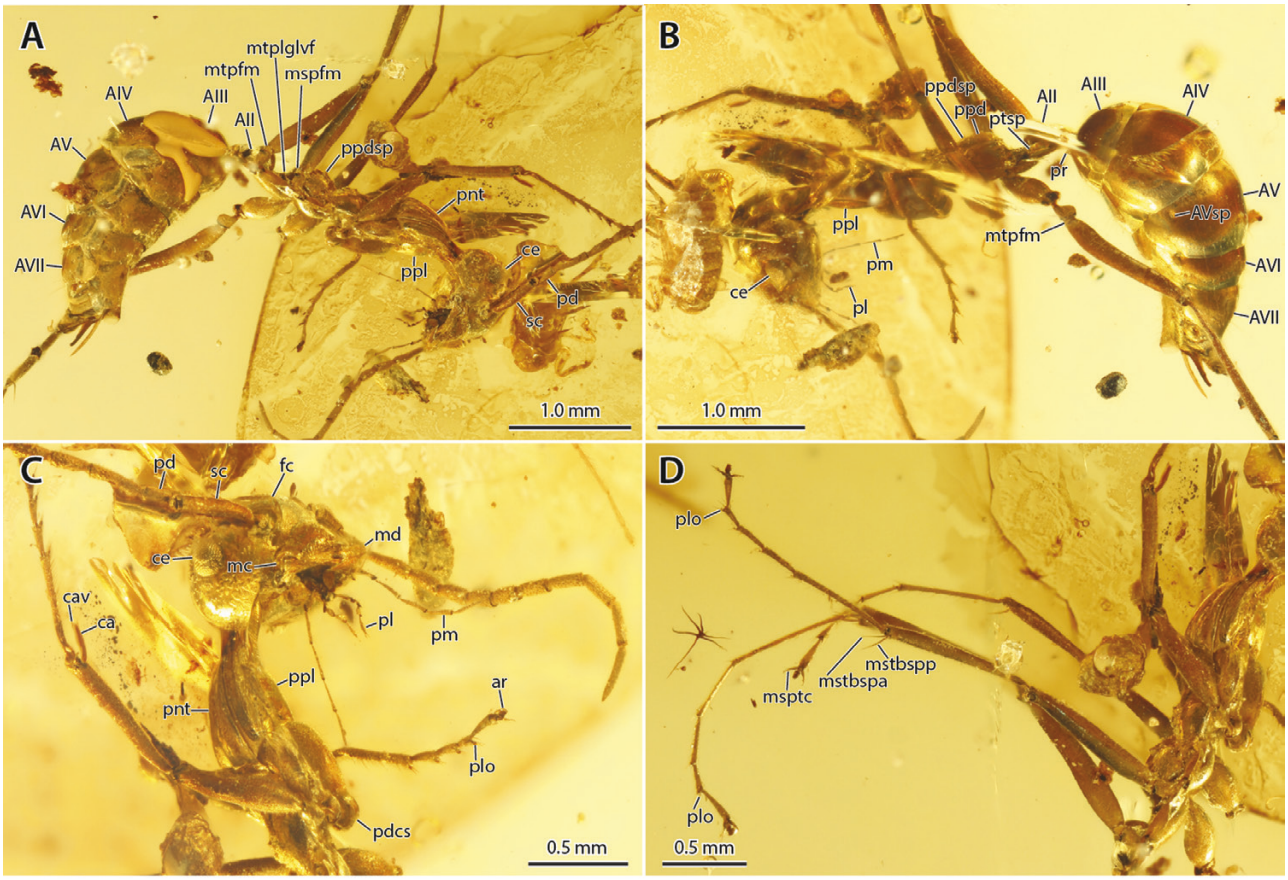

Figure 8. Photomicrographs of †*G. gracilis* showing setation and certain key features. Specimen CASENT0741232. A, body in ventrolateral anterior oblique view. B, body in dorsolateral posterior oblique view. C, detail of head and prothorax in ventrolateral anterior oblique view. D, detail of mid and hind legs in ventrolateral anterior oblique view. Abbreviations: AII–VII, abdominal segments II–VII; AVsp, spiracle of abdominal segment V; ar, arolium; ca, calcar; cav, velum of calcar; ce, compound eye; fc, frontal carina; mc, cranial condyle of mandible; md, mandible; mspfm, prefemur of mesothoracic leg; msptc, tooth of mesothoracic leg pretarsal claw; mstbspa, anterior tibial spur of mesothoracic leg; mstbspp, posterior tibial spur of mesothoracic leg; mtpfm, prefemur of metathoracic leg; mtplglvf, metapleural gland ventral flange; pd, pedicel; pdcs, prodisticoxal suture; pl, labial palp; plo, plantar lobe; pm, maxillary palp; pnt, pronotum; ppd, propodeum; ppdsp, propodeal spiracle; ppl, propleuron; pr, prora; ptsp, spiracle of the petiole; sc, scape.

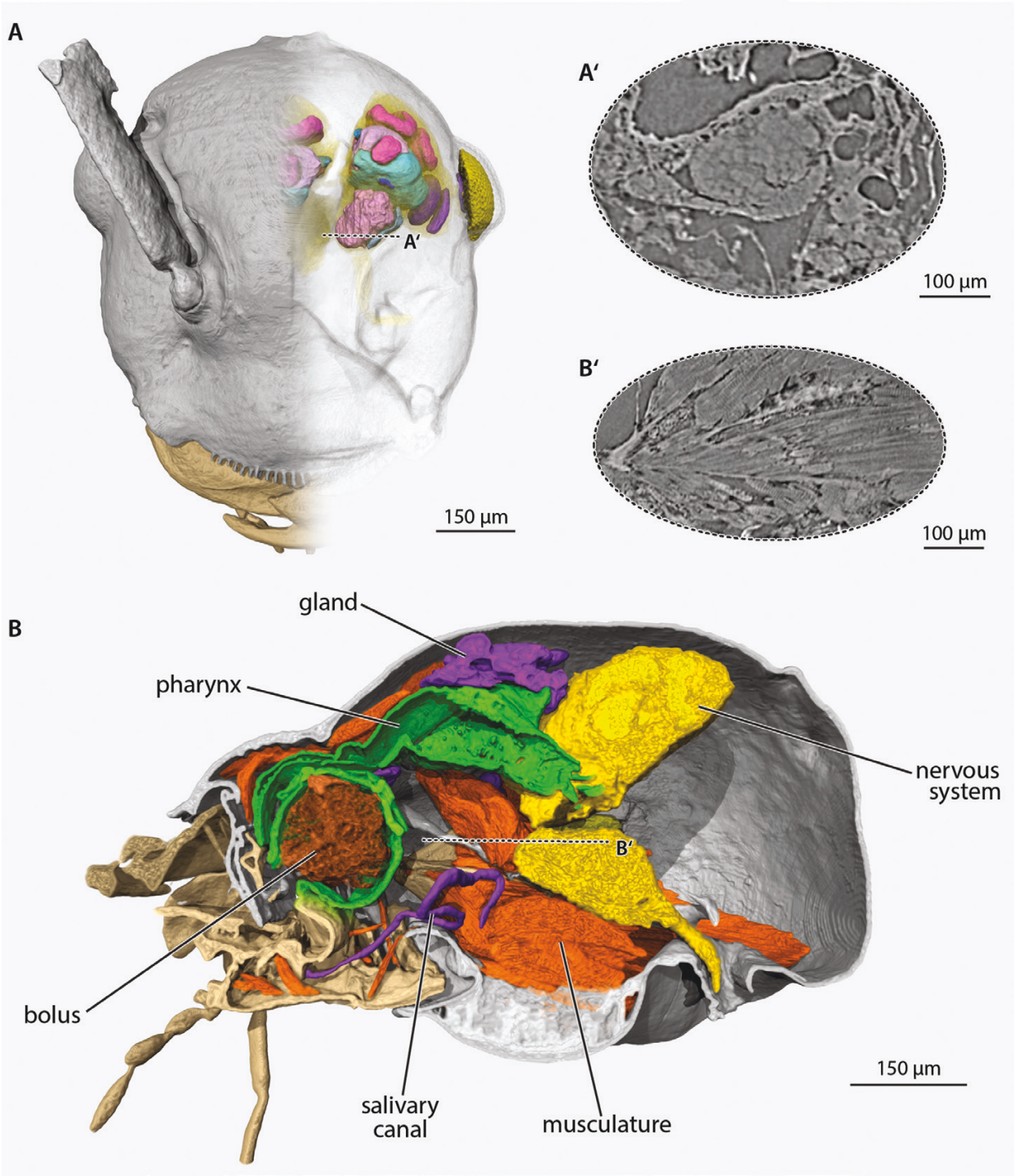

Figure 9. Exceptional soft tissue preservation. The adult specimen of †*G. gracilis* displays exceptional preservation of soft tissues, including identifiable neuropils (A), countable glomeruli of the antennal lobe (A'), the digestive tract, glands, and muscle (B), down to the scale of individual muscular cross-striations (B').

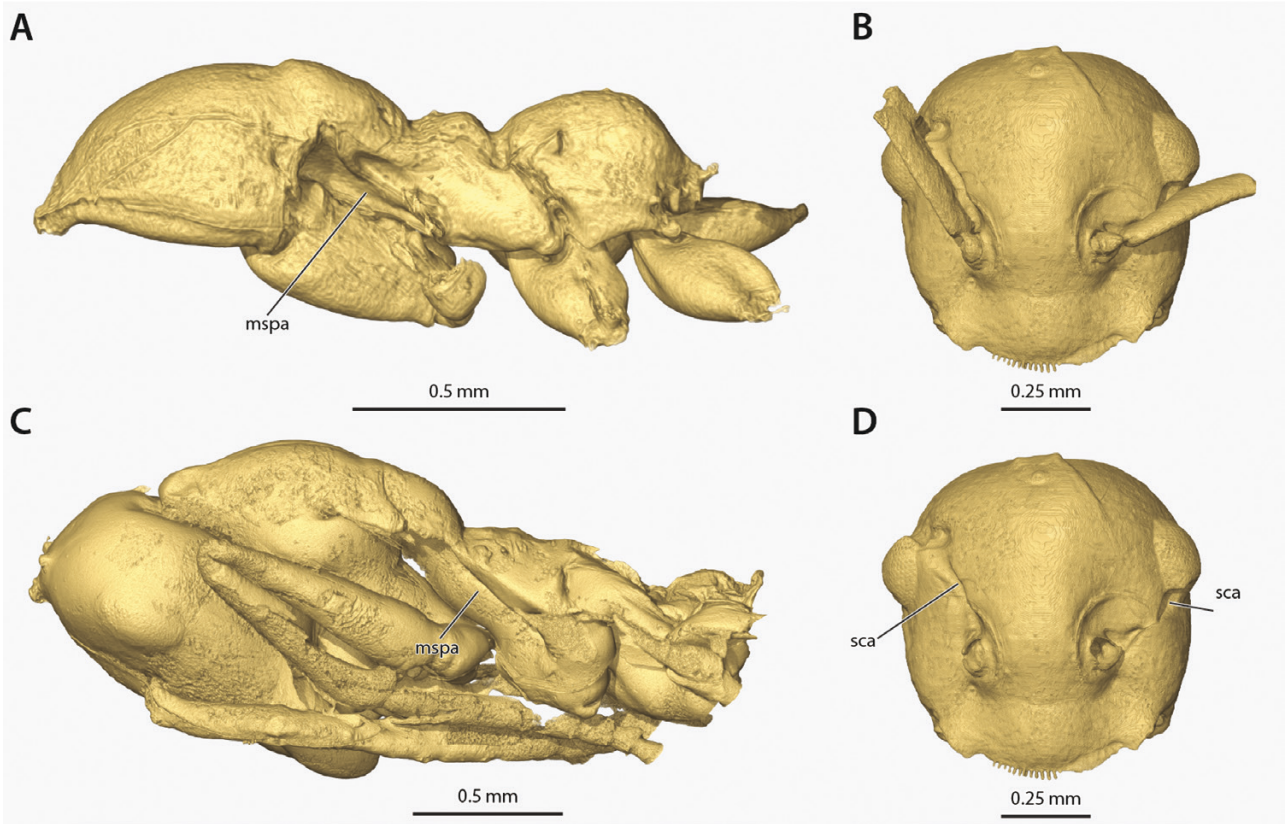

Figure 10. Features hidden by appendages, including artefacts caused by close proximity of limbs. †*Gerontoformica gracilis*: A, B, D, adult, CASENT0741232; C, pupa (CASENT0741231). A, C, mesosoma in lateral view with the legs distal to the coxae digitally removed, with the exception of the fore leg of (C), which is not cropped from the render. B, D, head in facial view with the scapes digitally rendered (B) and removed (D). Abbreviations: mspa, mesopectal artefact; sca, scapal artefact.

ants. Micro-computed tomography (μ-CT) not only uncovered exceptional preservation, including internal soft-tissues (Fig. 8), but also that the wingless females represented two distinct species, †*G. sternorhabda* and †*G. gracilis*. Therefore, we conducted a three-dimensional morphometric study which supports conspecificity of the pupa with the closely situated †*G. gracilis* adult (Supporting Information, Fig. S1, Dataset 1; Fig. 1A, B). Because ant pupae are immobile and the amber matrix is relatively free of debris, it is likely that the pupa was being transported at the time of capture. Brood transport is a derived social behaviour of ants relative to other stinging wasps, and thus provides the best evidence for cooperative brood care (Fig. 3A), substantiating the hypothesis that wingless adult stem ants were nurses as well as hunters, thus were workers. In other words, this fossil provides the final necessary support for the inference that the stem ants were indeed obligately eusocial, as previously hypothesized (e.g. Wilson *et al.*, 1967a, b; Perrichot *et al.*, 2008; Barden & Grimaldi, 2016).

Morphological re-evaluation of the complete fossil record of the stem ants (Supporting Information, Fig. S1, Dataset 2) reveals that winged–wingless polyphenism may have been an ancestral condition of the total clade Formicidae (Fig. 3A), so far as is known. The evolution of this polyphenism is expected to facilitate cooperative brood care through decreasing the dispersal capacity of some individuals (Wilson, 2008; Nowak *et al.*, 2010), while also increasing the potential for developmental canalization of worker-specific phenotypes (Wheeler, 1986). Morphological evidence further demonstrates that the transition to highly specialized wingless-specific (worker-like) phenotypes has evolved in parallel between the crown and stem ants. The most extreme example is in the †Zigrasimeciinae, where a completely fused and dome-shaped mesosomal phenotype has converged on the form of certain crown ant genera (Fig. 3C); the wingless individuals of these ants may also vary allometrically in body size (Cao *et al.*, 2020b). †Haidomyrmecinae, in contrast, display vestigial flight sclerites in wingless individuals (Fig.

KEY TO DESCRIBED †*GERONTOFORMICA* SPECIES

Note 1: This key excludes †*G. orientalis* nom. dub., †*G. rugosa* nom. dub. and †*G. tendir* nom. dub., which are presently considered to be unidentifiable. †*Gerontoformica cretacica* nom. dub. is keyed with †*G. occidentalis*, and †*G. spiralis* is keyed with †*G. subcuspis*; these latter two may yet be distinct but no discrete structural features were found to separate them.

Note 2: As the alpha taxonomy of †*Gerontoformica* is in need of revision, this key is expected to fail for certain well-preserved specimens that are undescribed, or which have not been accounted for in the current species-level circumscriptions. Therefore, we intend this key to be as morphologically concrete as possible, and we strongly recommend high-resolution µ-CT scanning for established type specimens, and for representatives of new taxa.

1. (Fig. 11-1): (1) Mesonotum *with* transverse ridge at about midlength, thus the mesonotal sclerite is divided into distinct mesoscutal and mesoscutellar areas; appearing distinctly angled in profile view. (2a) Abdominal segment IV (metasomal III) *cinctate*, i.e. with transverse sulci in their anterior halves, these distinctly separating the anterior surface (presclerite) which contacts the preceding sclerite from the remaining, exposed posterior surface (postsclerite). (2b) Abdominal segment III (metasomal II) *with* posterior margins constricted to some degree, in association with the formation of the cinctus. (3) Anteroventral process of abdominal segment III (prora) *conspicuous*, i.e. projecting ventrally and thick in appearance (anteroposteriorly wide in profile). (4) Standing setation on propodeum and petiolar tergum *long and conspicuous* (uncertain for †*G. contega*, sparser on other body regions in †*G. sternorhabda*). (5) Kachin amber ..... 2 (*pilosa* species group)

- Fig. 11-1': (1) Mesonotum *without* transverse ridge, thus the mesonotal sclerite is undivided, appearing flat or convex without distinct angle in profile view. (2a) Abdominal segment IV *not cinctate*, i.e. without transverse sulci in their anterior halves, thus the anterior contact surfaces of the tergum and sternum are continuous with the posterior surfaces which can be overlapped. (2b) Abdominal segment III *with* posterior margins not constricted. (3) Anteroventral process of abdominal segment III *inconspicuous*, i.e. projecting anteriorly and narrow in profile. (4) Standing setation on body *inconspicuous*. (5) Kachin or Charentese amber 5

2. Fig. 12-2: (1) Anteroventral process of petiolar sternum (subpetiolar process) *longer* dorsoventrally than anteroposteriorly wide, long and more-or-less digitate in form. (2) Head lateromedially *broader* than anteroposteriorly long in full-face view. (3) Transverse sulci of abdominal segment IV *weakly impressed*; that of the sternum more heavily impressed than that of tergum. (4) Teeth of pretarsal claws *strongly reduced*. (5) Body *small*; mesosoma length < 1.5 mm ..... †*G. sternorhabda* sp. nov.

- Fig. 12-2': (1) Anteroventral process of petiolar sternum *shorter* dorsoventrally than anteroposteriorly wide, low and subtriangular in form. (2) Head lateromedially *narrower* than anteroposteriorly long in full-face view. (3) Transverse sulci of abdominal segment IV *deeply impressed*; degree of impression between tergum and sternum not discernibly distinct. (4) Teeth of pretarsal claws *distinctly developed*. (5) Body *large*; mesosoma length > 1.5 mm 3

3. Fig. 13-3: (1) Anteroventral process of abdominal segment III *conspicuous*, *shark-fin-like* in form, i.e. approximately in the form of an equilateral triangle with the anterior margin weakly curved in profile view, and with its length about 0.5 × that of the petiolar sternum. (2) Abdominal segment III *long and anteriorly thin*, with the anteroposterior length of its postsclerites about equal to their dorsoventral height ..... †*G. pilosa* (Barden & Grimaldi, 2014)

- Fig. 13-3': (1) Anteroventral process of abdominal segment III less conspicuous (*of unknown form!*). (2) Abdominal segment III *tall and anteriorly thick*, with the anteroposterior length of its postsclerites shorter than their dorsoventral height 4

4. Fig. 14-4: (1) Body *large*; mesosoma length > 2.5 mm. (2) Scapal scrobe on face *short*, pit-like, not extending to compound eye .....†*G. magna* (Barden & Grimaldi, 2014)

- Fig. 14-4': (1) Body *smaller*; mesosoma length < 2.0 mm. (2) Scapal scrobe on face *long*, canal-like, extending to compound eye (*note*: could only be observed from left side, thus symmetry not confirmed, i.e. possibly artefactual).....†*G. contega* (Barden & Grimaldi, 2014)

5. Fig. 15-5: (1) Petiolar node dorsoventrally *taller* than anteroposteriorly long, appearing subsquamiform in profile view. (2) From Charentese (French) amber *cretacica* species group [*either* †*G. cretacica* Nel & Perrault, 2004 nom. dub. *or* †*G. occidentalis* (Perrichot *et al.*, 2008)]

- Fig. 15-5': (1) Petiolar node anteroposteriorly *longer* than dorsoventrally tall, appearing more-or-less wedge-shaped in profile view. (2) From Kachin (Burmese/Myanmarese) amber ... 6 (*gracilis* species group)

6. Fig. 16-6: (1) Mesosoma *boxy* in overall appearance; both mesonotum and metanotum are flattened and forming an almost even, linear slope that is only interrupted by the mesometanotal sulcus in lateral view .....†*G. robusta* (Barden & Grimaldi, 2014)

- Fig. 16-6': (1) Mesosoma *lumpy* in overall appearance; both mesonotum and metanotum are separate and convex, forming a pair of dorsal bulges between the pronotum and propodeum 7

7. Fig. 17-7: (1) Mesometanotal and metanotopropodeal sulci anteroposteriorly *broad*; breadth of these sulci greater than the diameter of the meso- or metabasitarsi. (2) Propodeal spiracle *with* an anterior flange .....†*G. gracilis* (Barden & Grimaldi, 2014)

- Fig. 17-7': (1) Mesometanotal and metanotopropodeal sulci anteroposteriorly *narrow*; breadth of these sulci less than the diameter of the meso- or metabasitarsi. (2) Propodeal spiracle *without* an anterior flange .....*either* †*G. spiralis* (Barden & Grimaldi, 2014) *or* †*G. subcuspis* (Barden & Grimaldi, 2014)

3B), and the †Sphecomyrminae display a trend toward wingless-specific, worker-like phenotypes (Supporting Information, Fig. S1, Dataset 2). Determining whether ants passed through a period of obligate monogamy (Boomsma & Gawne, 2018) or not (Olejarz *et al.*, 2015) is unanswerable with fossils. However, through µ-CT analysis of internal genital tissue, it may be possible to determine the evolutionary sequence of female diphenism and reproductive sterility (Khila & Abouheif, 2010) from the fossil record. Such study may also refine our understanding of the evolution of ergatoid queens, i.e. wingless reproductive females, which can coexist with permanent workers, or of gamergates, i.e. mated and sexually reproducing worker ants (Peeters, 2012).

The holotype (AMNH Bu-SY23) is the second described syninclusion of two ant species from Cretaceous amber, which has been previously recorded for the genus †*Gerontoformica* (Barden & Grimaldi, 2014). These two fossils indicate that individuals of different †*Gerontoformica* species must have significantly interacted, and that they were relatively numerous, despite the fact that ants do not make up as large a proportion of the entomofauna of this time (LaPolla *et al.*, 2013; Barden, 2017; Barden & Engel, 2020). Moreover, our morphological comparisons, based on the highest resolution scans of stem ants to date, suggest that †*Gerontoformica* were ecologically diverse, despite being comparatively 'generalized' relative to other stem groups (e.g. Barden & Grimaldi, 2016; Barden *et al.*, 2020; Boudinot *et al.*, 2020b; Cao *et al.*, 2020c). Specifically, we observed two discrete attachment strategies for locomotion, with †*G. sternorhabda* having brushy, plantula-less tarsi with small arolia, and †*G. gracilis* having comparatively bald, planta-bearing tarsi with much larger arolia. Among extant ants, the hairy tarsi of *Daceton* Perty, 1833, *Formica* Linnaeus, 1758 and *Oecophylla* F.Smith, 1860 enable these ants to adhere to steeply sloping surfaces and perhaps carry load without toppling (Endlein & Federle, 2015; Billen *et al.*, 2017; Wöhrl *et al.*, 2021), while large aroliae are critical for smooth-surface attachment (Orivel *et al.*, 2001). Therefore, †*Gerontoformica sternorhabda* and †*G. gracilis* may have preferred different surfaces and occupied distinct niches within the same habitat. Further attention on the tarsal morphology of stem ants is certainly warranted for both systematic and functional studies.

Finally, from the taxonomic perspective, our reorganization of †*Gerontoformica* highlights the need for a deeper systematic revision of the genus, ideally incorporating numerous specimens and

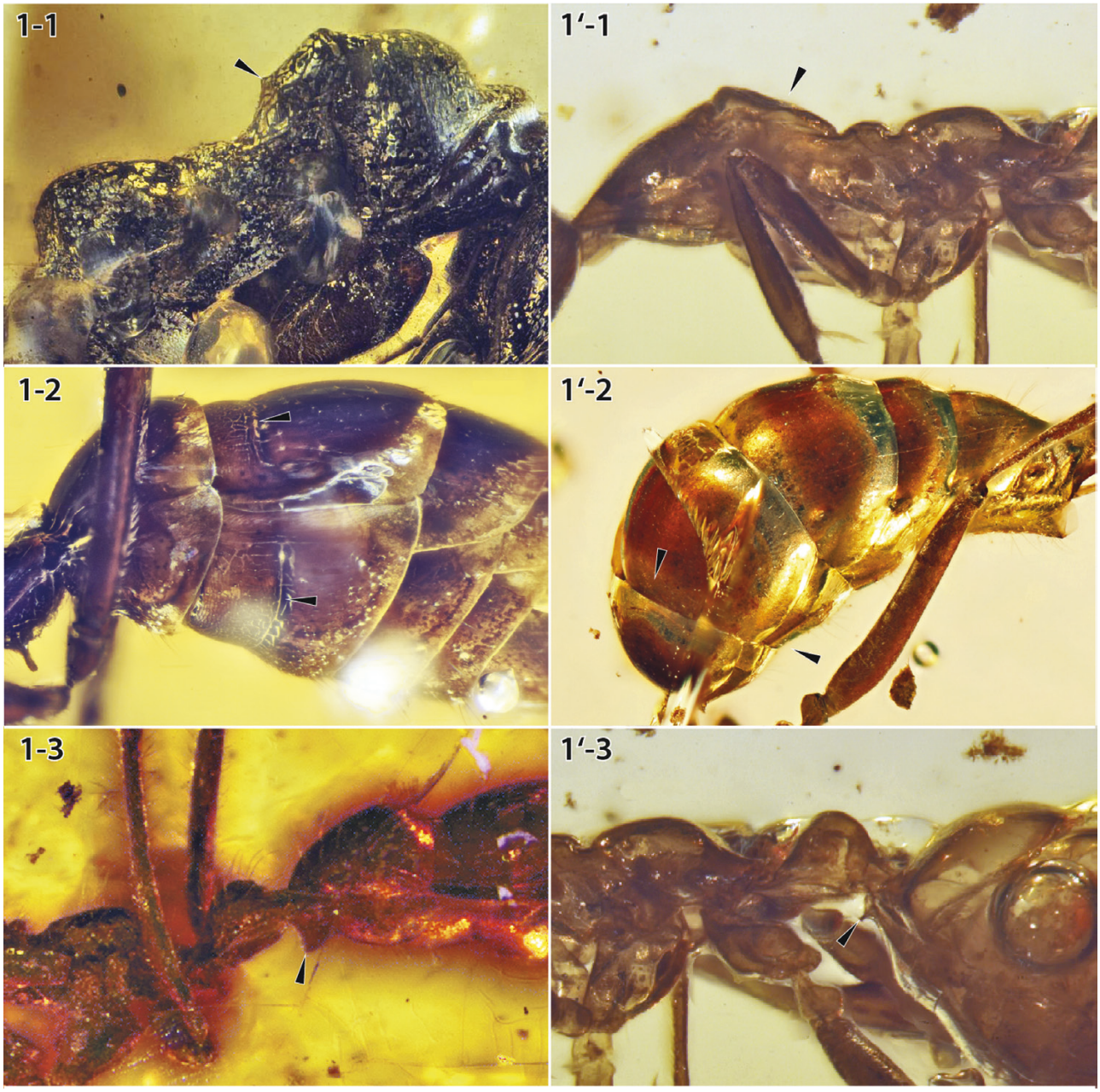

Figure 11. Couplet 1: mesonotum with (1-1) or without (1'-1) transverse ridge; abdominal segment IV with (1-2) or without (1'-2) cinctus; prora large (1-3) or small (1'-3). (1-1) †*G.* ufv-05, ANTWEB103848 (J. Chaul, AntWeb), mesosoma in profile view. (1'-1, 1'-3) †*G.* indet., JWJ-Bu19 (V. Perrichot, AntWeb), mesosoma in profile view. (1-2) †*G. sternorhabda* sp. nov. paratype, UFV-LABECOL-009656, metasoma in ventrolateral view. (1'-2) †*G. gracilis*, CASENT0741232, metasoma in lateral view. (1-3) †*G. pilosa* holotype, JZC-Bu225 (P. Barden, AntWeb), anterior metasoma in profile view.

employing μ-CT. Although the four species we recognize as *nomina dubia* may not be resolved, it is possible to petition the International Commission for Zoological Nomenclature to employ its plenary powers to set aside these types so that neotypes may be chosen (section 75.5 of the ICZN, 2021), should adequate specimens of these species be found. Furthermore, we are aware of additional material that will require the erection of new species, and we strongly recommend μ-CT scanning of all previously (and newly) designated holotypes. We consider the latter point to be important because the renders allow for the study of three-dimensional structural form, and they reveal greater structural detail and

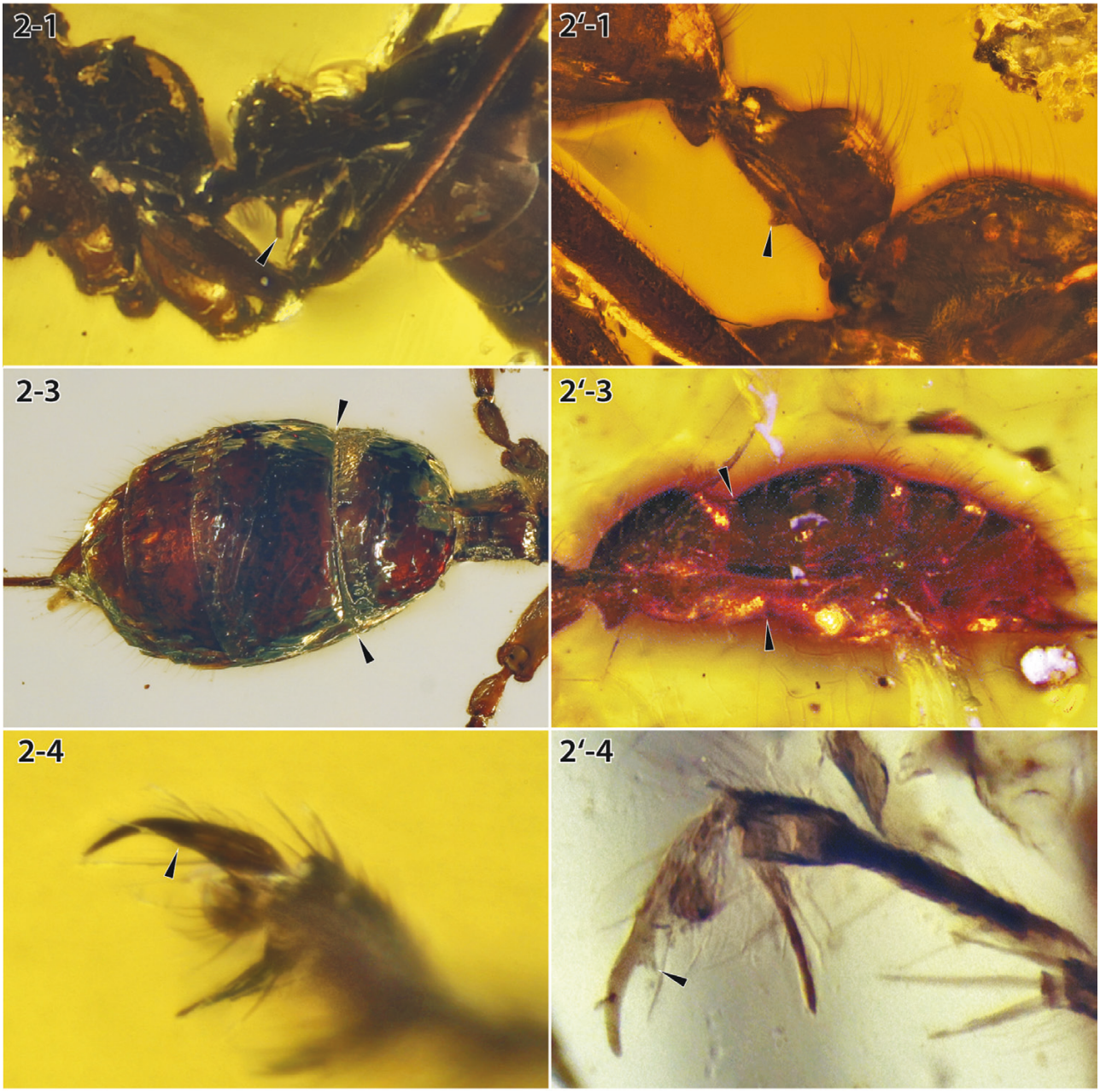

Figure 12. Couplet 2: subpetiolar process long and narrow (2-1) or short and wide (2'-1); abdominal segment IV with weak (2-3) or strong (2'-3) constriction; and pretarsal claw subapical teeth strongly reduced (2-4) or well developed (2'-4). (2-1, 2-4) †*G. sternorhabda* sp. nov. paratype, UFV-LABECOL-009656, petiole in lateral view (2-1) and pretarsal claw in distal oblique view (2-4). (2'-1) †*G. pilosa* ANTWEB1038931 (M. Baldi, AntWeb), petiole in dorsolateral oblique view. (2-3) †*G. sternorhabda* sp. nov. paratype, CASENT0741234, metasoma in dorsolateral oblique view. (2'-3) †*G. pilosa* holotype, JZC-Bu225 (P. Barden, AntWeb), metasoma in profile view. (2'-4) †*G. pilosa* species group indet., ANTWEB1041010 (J. Chaul, AntWeb), pretarsal claw in distal oblique view.

features that are concealed, including internal and soft-tissue anatomy. Scans of the previously described †*Gerontoformica* holotypes will be critical for evaluating structures that have been heretofore undescribed, such as the subapical processes of the proximal labial palpomeres, and for determining whether certain features are artefacts or true phenotypic expressions. Our hope with the present

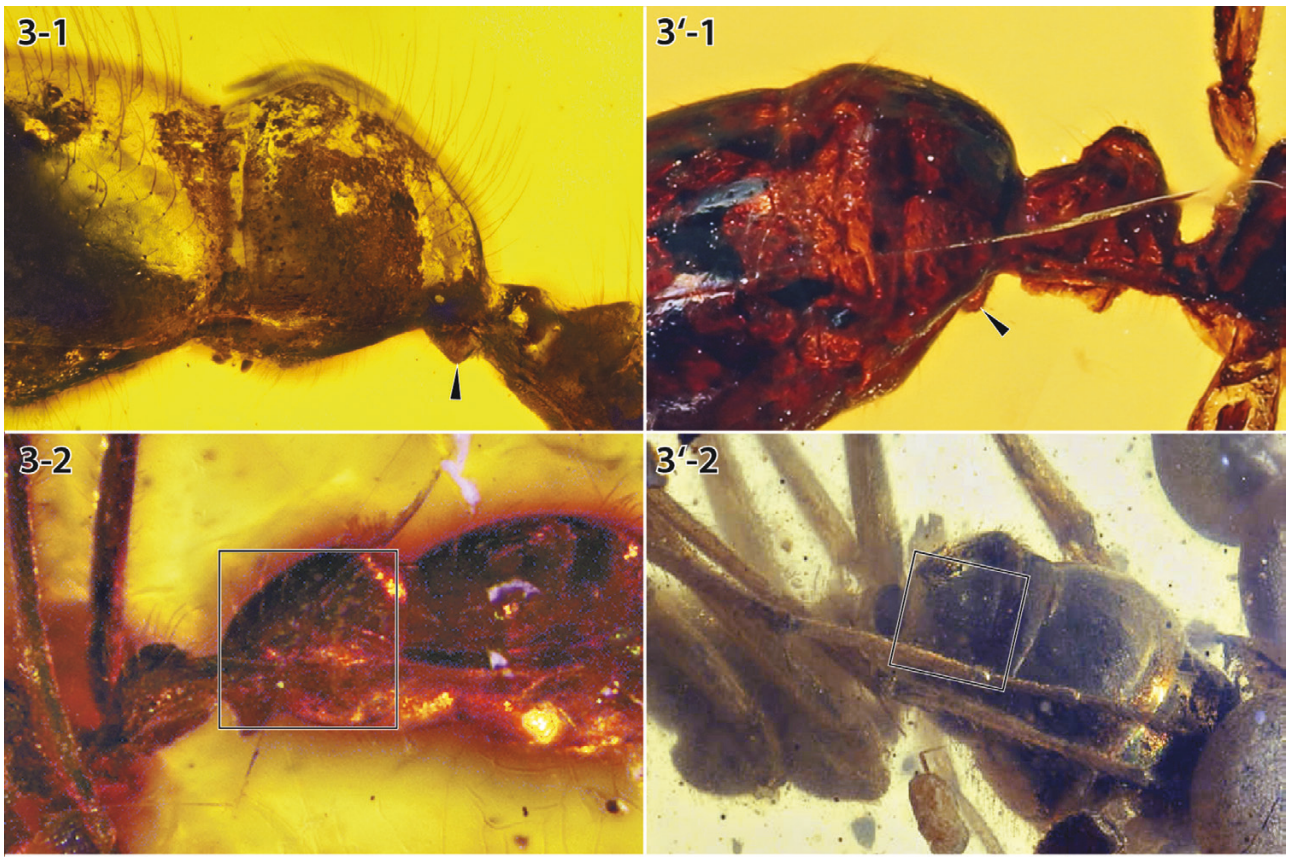

Figure 13. Couplet 3: prora large and triangular (3-1) or smaller and of a different shape (3’-1); abdominal segment III about as long as tall (3-2) or taller than long (3’-2). (3-1) †*G. pilosa* ANTWEB1038931 (M. Baldi, AntWeb), abdominal segment III in dorsolateral oblique view. (3’-1) †*G. sternorhabda* sp. nov. holotype, CASENT0741233, abdominal segment III in dorsolateral oblique view. (3-2) †*G. pilosa* holotype, JZC-Bu225 (P. Barden, AntWeb), abdominal segment III in lateral view. (3’-2) †*G. magna*, FANTWEB00014 (V. Perrichot, AntWeb), abdominal segment III in dorsolateral oblique view.

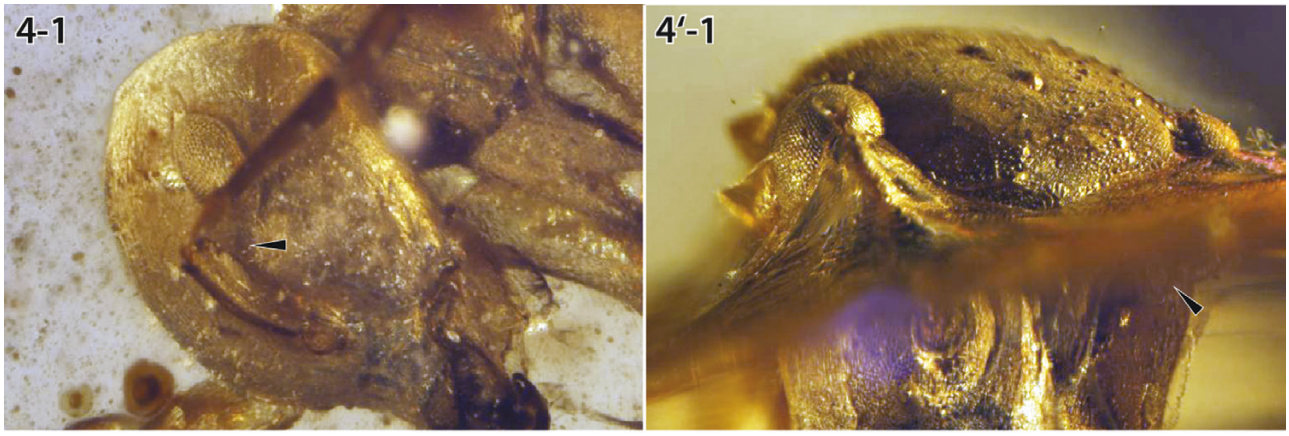

Figure 14. Couplet 4: antennal scrobe reaching (4-1) or not reaching (4’-1) compound eye. (4-1) †*G. contega* holotype, JZC-Bu300 (P. Barden, AntWeb), head in oblique lateral view. (4’-1) †*G. magna* holotype, JZC-Bu108 (P. Barden, AntWeb), head in oblique facial view.

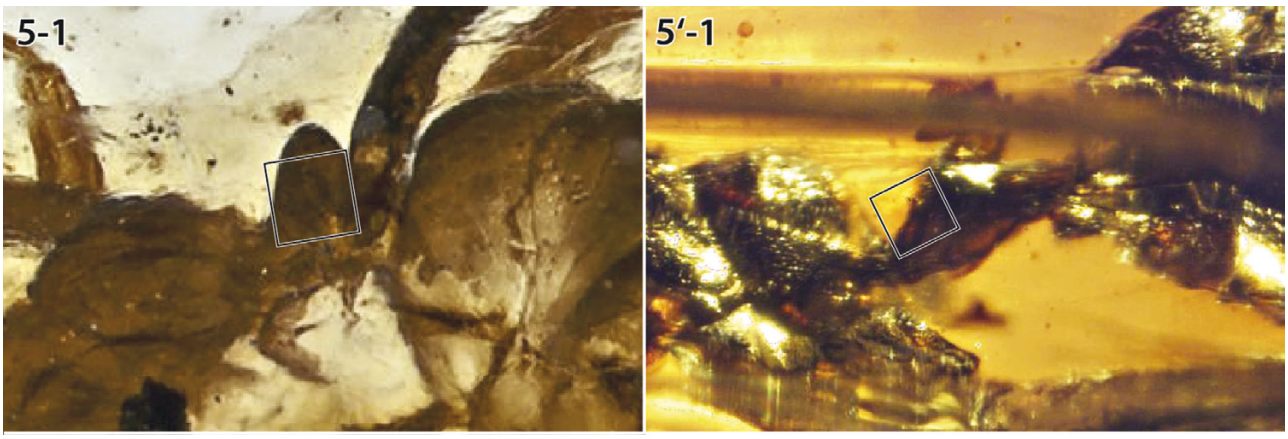

Figure 15. Couplet 5: petiolar tergum taller than long (5-1) or longer than tall (5'-1). (5-1) †*G. occidentalis* paratype, MNHN-A30166 (V. Perrichot, AntWeb), petiole in dorsolateral oblique view. (5'-1) †*G. subcuspis* holotype, JZC-Bu304 (P. Barden, AntWeb), petiole in lateral view.

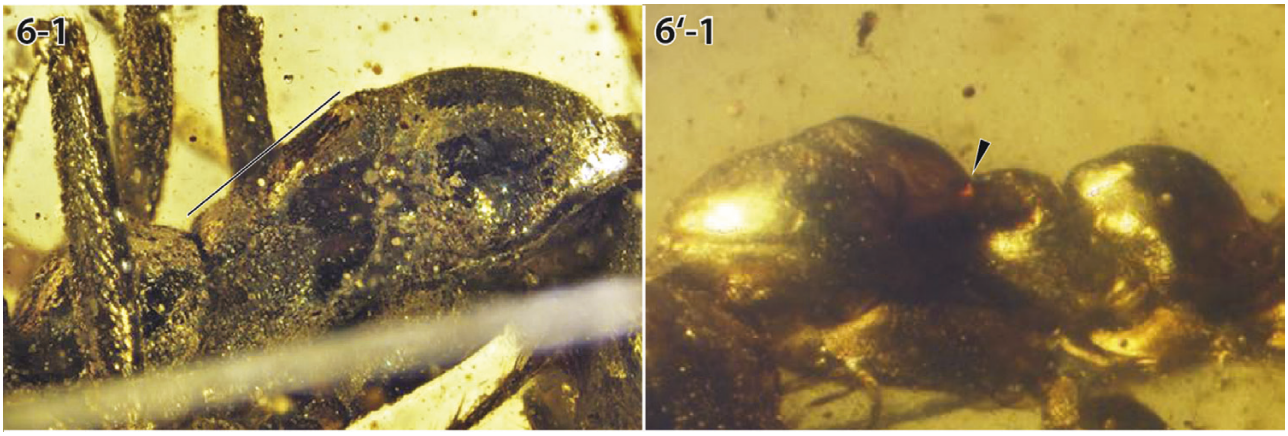

Figure 16. Couplet 6: meso- and metathorax forming continuous slope (6-1) or a pair of bulges (6'-1). (6-1) †*G. robusta* holotype, JZC-Bu223 (P. Barden, AntWeb), mesosoma in lateral view with anterior to the right. (6'-1) †*G. spiralis* holotype, JZC-Bu222 (P. Barden, AntWeb), mesosoma in lateral, anterodorsally oblique view, with anterior to the left.

key and descriptions is to guide future work on the genus, which we consider to be highly desirable.

CONCLUSIONS

The synincluded, conspecific adult and pupa adduced here substantiate the hypothesis that wingless female stem ants were cooperators, hence true workers, and that stem ants were indeed obligately eusocial. After re-examination of all described Mesozoic ants, the coexistence of stem taxa on a spectrum of inter-caste derivation was revealed, which strongly supports the Early Cretaceous, or perhaps earlier, as the 'Axial Age' of eusociality for the total clade of the ants and termites (see also, e.g. Engel *et al.*, 2016). While our work effectively pushes the origin of eusociality deeper into geological time for ants, our µ-CT scans reveal a new avenue of research: palaeosociobiology. Specifically, our µ-CT data revealed exceptional and unexpected soft-tissue preservation in the head (Fig. 9), including the nervous system and individually identifiable muscles and glands, indicating that evaluation of ovariole count and spermatheca development might be possible in other fossil ants. Did the evolution of winged–wingless diphenism precede the substantial reduction of fertility, was loss of normal reproductive capacity first or, did both evolve simultaneously? *Vis à vis* the extreme winged–wingless diphenism of †*Zigrasimecia*, we ask: could it be possible that total worker sterility also evolved in stem ants? Our discovery and analysis sheds light on the evolution of eusociality through confirmation of

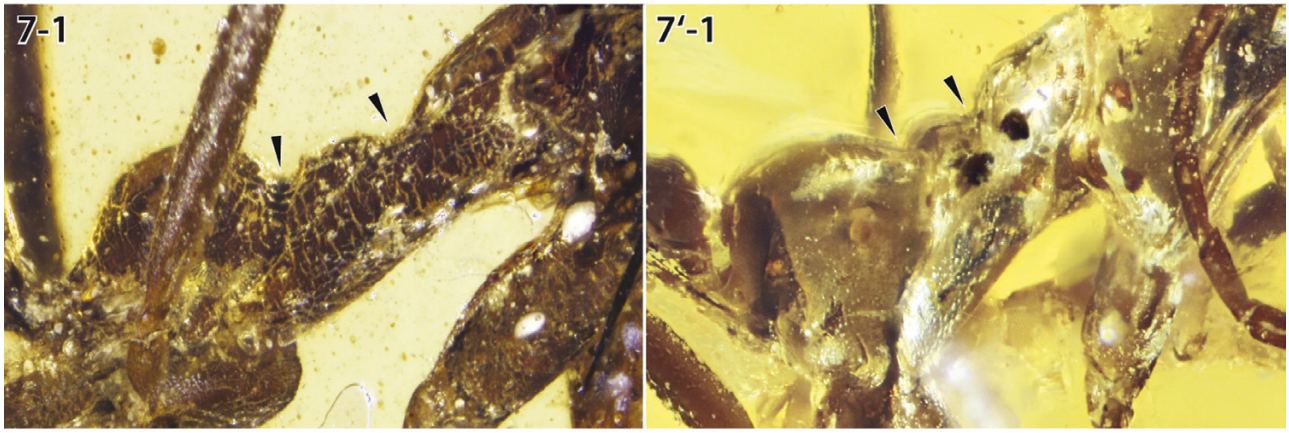

Figure 17. Couplet 7: transverse sulci of mesosoma broad (7-1) or narrow (7'-1). (7-1) †*G. gracilis* holotype, JZC-Bu324 (P. Barden, AntWeb), mesosoma in lateral view. (7'-1) †*G. gracilis* group indet., ANTWEB1032529 (J. Chaul, AntWeb), mesosoma in lateral view.

worker cooperation and by revealing underappreciated mesosomal variation in ants, indicating new potential to illuminate the evolutionary patterns of Darwin's 'one special difficulty': the superorganism.

ACKNOWLEDGEMENTS

We thank D. Grimaldi and C. Richenbacher for access to the AMNH. We also thank P. Barden and V. Perrichot for collegial support and their critical and ongoing efforts to document the ant fossil record. P. Barden also provided helpful discussion during the revision process of this manuscript. For discussion about the definitions of eusociality and for critical commentary, BEB thanks J. Shik and J. Boomsma (University of Copenhagen) and D. Kronauer and his research group (Rockefeller University). We further thank R. Rajakumar (University of Ottawa) for stimulating our interest in and understanding of caste development in ants. Finally, we thank the Imaging Section of the Research Support Division at OIST for supporting the CT scanning setup. BEB was supported by an Alexander von Humboldt Research Fellowship; JCMC by the Brazilian funding agencies CAPES and CNPQ; AR by an Evangelisches Studienwerk Villigst eV scholarship; and SY by a Grant-in-Aid for JSPS Fellows (20J00159) from the Japan Society for the Promotion of Science (JSPS), Tokyo, Japan.

AUTHOR CONTRIBUTIONS

Designed research: BEB, AR, JK, RAK, EPE, RGB, SY. Performed research: BEB, AR, JK, JCMC, SY. Contributed analytic tools: RGB, EPE. Microphotography: JCMC, SY. Analysed data: BEB, AR, JK, JCMC. Performed µ-CT: JK. Processed µ-CT data: AR. Post-processed µ-CT data: AR, BEB. Wrote manuscript: BEB. Revised manuscript: BEB, AR, JK, JCMC, RAK, EPE, RGB, SY.

DATA AVAILABILITY

The µ-CT datasets used herein are available at Zenodo, accessible with the following doi: 10.5281/zenodo.5608454. In addition, we provide freely accessible 3D models of the two scanned species on Sketchfab (†G. sternorhabda sp. n.: https://sketchfab.com/3d-models/casent0741233-gerontoformica-sternorhabda-df7a9eb558bd43d09e99ad3555b8dfa0) and (†G. gracilis: https://sketchfab.com/3d-models/casent0741232-gerontoformica-gracilis-5f52c71ace5e418ea4f12924162536eb).

REFERENCES

AntWeb. 2021. AntWeb, v.8.55.2. California Academy of Sciences. Available at: https://www.antweb.org. (accessed 13 April 2021).

Balashov I. 2021. The first records of mollusks from mid-Cretaceous Hkamti amber (Myanmar), with the description of a land snail, *Euthema myanmarica* n. sp. (Caenogastropoda, Cyclophoroidea, Diplommatinidae). *Journal of Paleontology* **95:** 994–1003.

Barden P. 2017. Fossil ants (Hymenoptera: Formicidae): ancient diversity and the rise of modern lineages. *Myrmecological News* **24:** 1–30.

Barden P, Engel MS. 2020. Fossil social insects. In: Starr C, ed. *Encyclopedia of social insects*. Cham: Springer.

Barden P, **Grimaldi D. 2014.** A diverse ant fauna from the mid-Cretaceous of Myanmar (Hymenoptera: Formicidae). *PLoS One* **9:** e93627.

Barden P, **Grimaldi D. 2016.** Adaptive radiation in socially advanced stem-group ants from the Cretaceous. *Current Biology* **26:** 1–7.

Barden P, **Herhold HW**, **Grimaldi DA. 2017.** A new genus of hell ants from the Cretaceous (Hymenoptera: Formicidae: Haidomyrmecini) with a novel head structure. *Systematic Entomology* **42:** 837–846.

Barden P, **Perrichot V**, **Wang B. 2020.** Specialized predation drives aberrant morphological integration and diversity in the earliest ants. *Current Biology* **30:** 3818–3824.

Barraclough TG. 2019. *The evolutionary biology of species*. Oxford: Oxford University Press, 288.

Batelka J, **Engel MS**, **Falin ZH**, **Prokop J. 2011.** Two new ripidiine species in Dominican amber with evidence of aggregative behavior of males 'frozen' in the fossil record (Coleoptera: Ripiphoridae). *European Journal of Entomology* **108:** 275–286.

Beutel RG, **Gorb SN. 2001.** Ultrastructure of attachment specializations of hexapods (Arthropoda): evolutionary patterns inferred from a revised ordinal phylogeny. *Journal of Zoological Systematics & Evolution Research* **39:** 177–207.

Beutel RG, **Richter A**, **Keller RA**, **Hita Garcia F**, **Matsumura Y**, **Economo EP**, **Gorb SN. 2020.** Distal leg structures of the Aculeata (Hymenoptera): a comparative evolutionary study of *Sceliphron* (Sphecidae) and *Formica* (Formicidae). *Journal of Morphology* **281:** 737–753.

Billen J, **Al-Khalifa MS**, **Silva RR. 2017.** Pretarsus structure in relation to climbing ability in the ants *Brachyponera sennaarensis* and *Daceton armigerum*. *Saudi Journal of Biological Science* **24:** 830–836.

Bolton B. 1994. *Identification guide to the ant genera of the world*. Cambridge: Harvard University Press, 222.

Bolton B. 2003. Synopsis and classification of Formicidae. *Memoirs of the American Entomological Institute* **71:** 1–370.

Boomsma JJ, **Gawne R. 2018.** Superorganismality and caste differentiation as points of no return: how the major evolutionary transitions were lost in translation. *Biological Reviews* **93:** 28–54.

Borowiec ML, **Moreau CS**, **Rabeling C. 2020.** Ants: phylogeny and classification. In: Starr C, ed. *Encyclopedia of social insects*. Cham: Springer.

Boudinot BE. 2015. Contributions to the knowledge of Formicidae (Hymenoptera, Aculeata): a new diagnosis of the family, the first global male-based key to subfamilies, and a treatment of early branching lineages. *European Journal of Taxonomy* **120:** 1–62.

Boudinot BE, **Khouri Z**, **Richter A**, **Van de Kamp T**, **Barden P**, **Perrichot V**, **Chaul JCM. 2020a.** Chapter II. The evolution of the ants: extinct ant sister-group illuminates eusociality origin and post-K/Pg persistence. In: Boudinot BE, *Systematic and evolutionary morphology: case studies on Formicidae, Mesozoic Aculeata, and hexapodan genitalia*. Ph. D. Thesis, University of California, Davis, 174–393.

Boudinot BE, **Perrichot V**, **Chaul JCM. 2020b.** †*Camelosphecia* gen. nov., lost ant-wasp intermediates from the mid-Cretaceous (Hymenoptera, Formicoidea). *ZooKeys* **1005:** 21–55.

Boudinot BE, **Beutel RG**, **Gorb SN**, **Polilov AA. 2021a.** Functional diversity of attachment and grooming structures is retained in all but the smallest insects. *Journal of Zoology* **313:** 99–113.

Boudinot BE, **Moosdorf OTD**, **Beutel RG**, **Richter A. 2021b.** Anatomy and evolution of the head of *Dorylus helvolus* (Formicidae: Dorylinae): patterns of sex- and caste-limited traits in the sausagefly and the driver ant. *Journal of Morphology* **282:** 1616–1658. Doi: 10.1002/jmor.21410.

Cao H, **Perrichot V**, **Shih C**, **Ren D**, **Gao T. 2020a.** A revision of *Haidomyrmex cerberus* Dlussky (Hymenoptera: Formicidae: Sphecomyrminae) from mid-Cretaceous Burmese amber. *Cretaceous Research* **106:** 104226.

Cao H, **Boudinot BE**, **Shih C**, **Ren D**, **Gao T. 2020b.** Cretaceous ants shed new light on the origins of worker polymorphism. *Science China Life Science* **63:** 1085–1088.

Cao H, **Boudinot BE**, **Wang Z**, **Miao X**, **Shih C**, **Ren D**, **Gao T. 2020c.** Two new iron maiden ants from Burmese amber (Hymenoptera: Formicidae: †Zigrasimeciini). *Myrmecological News* **30:** 161–173.

Dlussky GM. 1975. Formicidae taxonomy; Hymenoptera Apocrita of Mesozoic. *Transactions of the Palaeontological Institute Academy of Sciences of the USSR* **147:** 1–134.

Dlussky GM. 1983. A new family of Upper Cretaceous Hymenoptera: an 'intermediate link' between the ants and the scolioids. *Paleontologicheskii Zhurnal* **1983:** 65–78 [in Russian].

Dlussky GM. 1996. Ants (Hymenoptera: Formicidae) from Burmese amber. *Paleontological Journal* **30:** 449–454.

Dlussky GM. 1999. The first find of the Formicoidea (Hymenoptera) in the Lower Cretaceous of the Northern Hemisphere. *Paleontological Journal* **33:** 274–277.

Dlussky GM, **Brothers DJ**, **Rasnitsyn AP. 2004.** The first Late Cretaceous ants (Hymenoptera: Formicidae) from southern Africa, with comments on the origin of the Myrmicinae. *Insect Systematics & Evolution* **35:** 1–13.

Endlein T, **Federle W. 2015.** On heels and toes: how ants climb with adhesive pads and tarsal friction hair arrays. *PLoS One* **10:** e141269.

Engel MS, **Grimaldi DA. 2005.** Primitive new ants in Cretaceous amber from Myanmar, New Jersey, and Canada (Hymenoptera: Formicidae). *American Museum Novitates* **3485:** 1–23.

Engel MS, **Barden P**, **Riccio ML**, **Grimaldi DA. 2016.** Morphologically specialized termite castes and advanced sociality in the Early Cretaceous. *Current Biology* **26:** 522–530.

Giłka W, **Zakrzewska M**, **Lukashevich ED**, **Vorontsov DD**, **Soszyńska-Maj A**, **Skibińska K**, **Cranston PS. 2021.** Wanted, tracked down and identified: Mesozoic non-biting midges of the subfamily Chironominae (Chironomidae, Diptera). *Zoological Journal of the Linnean Society* **zlab020**. Doi:10.1093/zoolinnean/zlab020.

Grimaldi D, **Agosti D. 2000.** A formicine in New Jersey Cretaceous amber (Hymenoptera: Formicidae) and early evolution of the ants. *Proceedings of the National Academy of Sciences of the USA* **97:** 13678–13683.

Guo Y, **Shih C**, **Zhou D**, **Ren D**, **Zhao Y**, **Gao T. 2021.** The first worker-queen association for Cretaceous Formicidae: the winged caste of *Haidomyrmex cerberus*. *ZooKeys* **1048:** 69–78.

Gustafson GT, **Michat MC**, **Balke M. 2020.** Burmese amber reveals a new stem lineage of whirligig beetle (Coleoptera: Gyrinidae) based on the larval stage. *Zoological Journal of the Linnean Society* **189:** 1232–1248.

Hanna L, **Abouheif E. 2021.** The origin of wing polyphenism in ants: an eco-evo-devo perspective. *Current Topics in Developmental Biology* **141:** 279–336.

Heggen HP, **Birks HH**, **Heiri O**, **Grytnes J-A**, **Birks HJB. 2012.** Are fossil assemblages in a single sediment core from a small lake representative of total deposition of mite, chironomid, and plant macrofossil remains? *Journal of Paleolimnology* **48:** 669–691.

Hsiao Y, **Li Y**, **Ren D**, **Pang H. 2021.** Morphological phylogenetics provide new insights into the classification and evolution of fossil soldier beetles from Mid-Cretaceous Burmese amber (Coleoptera: Cantharidae). *Zoological Journal of the Linnean Society* **zlaa184**. Doi:10.1093/zoolinnean/zlaa184.

ICZN. 2021. *The International code of zoological nomenclature, 4th edn*. Available at: iczn.org/the-code/the-code-online (accessed 28 June 2021).

Johnson BR, **Borowiec ML**, **Chiu JC**, **Lee EK**, **Atallah J**, **Ward PS. 2013.** Phylogenomics resolves evolutionary relationships among ants, bees, and wasps. *Current Biology* **23:** 2058–2062.

Jouault C, **Ngô-Muller V**, **Pouillon J-M**, **Nel A. 2021a.** New Burmese amber fossils clarify the evolution of bethylid wasps (Hymenoptera: Chrysidoidea). *Zoological Journal of the Linnean Society* **191:** 1044–1058.

Jouault C, **Maréchal A**, **Condamine FL**, **Wang B**, **Nel A**, **Legendre F**, **Perrichot V. 2021b.** Including fossils in phylogeny: a glimpse into the evolution of the superfamily Evanioidea (Hymenoptera: Apocrita) under tip-dating and the fossilized birth–death process. *Zoological Journal of the Linnean Society* **zlab034**. Doi: 10.1093/zoolinnean/zlab034.

Keller RA. 2011. A phylogenetic analysis of ant morphology (Hymenoptera: Formicidae) with special reference to the poneromorph subfamilies. *Bulletin of the American Museum of Natural History* **355:** 1–90.

Khila A, **Abouheif E. 2010.** Evaluating the role of reproductive constraints in ant social evolution. *Philosophical Transactions of the Royal Society B* **365:** 617–630.

LaPolla JS, **Dlussky GM**, **Perrichot V. 2013.** Ants and the fossil record. *Annual Review of Entomology* **58:** 609–630.

Latreille PA. 1809. *Genera crustaceorum et Insectorum secondum ordinem naturalem in familias disposita iconibus exemplisque plurimus explicata. Tomus 4*. Paris and Strasbourg: A. Koenig, 399.

Liu S-P, **Richter A**, **Stoessel A**, **Beutel RG. 2018**. The mesosomal anatomy of *Myrmecia nigrocincta* workers and evolutionary transformations in Formicidae (Hymenoptera). *Arthropod Systematics & Phylogeny* **77:** 1–19.

Mao Y, **Liang K**, **Su Y**, **Li J**, **Rao X**, **Zhang H**, **Xia F**, **Fu Y**, **Cai CH**, **Huang D. 2018.** Various amber ground marine animals on Burmese amber with discussions on its age. *Palaeoentomology* **1:** 91–103.

McKellar RC, **Glasier JRN**, **Engel MS. 2013.** A new trap-jawed ant (Hymenoptera: Formicidae: Haidomyrmecini) from Canadian Late Cretaceous amber. *The Canadian Entomologist* **145:** 454–465.

McKenna KZ, **Wagner GP**, **Cooper KL. 2021.** A developmental perspective of homology and evolutionary novelty. *Current Topics in Developmental Biology* **141:** 1–38.

Miao Z, **Wang M. 2019.** A new species of hell ants (Hymenoptera: Formicidae: Haidomyrmecini) from the Cretaceous Burmese amber. *Journal of the Guangxi Normal University (Natural Science Edition)* **37:** 139–142.

Nel A, **Perrault G**, **Perrichot V**, **Néraudeau D. 2004.** The oldest ant in the Lower Cretaceous amber of Charente-Maritime (SW France) (Insecta: Hymenoptera: Formicidae). *Geologica Acta* **2:** 23–29.

Nowak MA, **Tarnita CE**, **Wilson EO. 2010.** The evolution of eusociality. *Nature* **466:** 1057–1062.

Olejarz JW, **Allen B**, **Veller C**, **Nowak MA. 2015.** The evolution of non-reproductive workers in insect colonies with haplodiploid genetics. *eLife* **4:** e08918.

Orivel J, **Malherbe MC**, **Dejean A. 2001.** Relationships between pretarsus morphology and arboreal life in ponerine ants of the genus *Pachycondyla* (Formicidae: Ponerinae). *Annals of the Entomological Society of America* **94:** 449–456.

Peeters C. 2012. Convergent evolution of wingless reproductives across all subfamilies of ants, and sporadic loss of winged queens (Hymenoptera: Formicidae). *Myrmecological News* **16:** 75–91.

Peris D, **Jelínek J. 2020.** Syninclusions of two new species of short-winged flower beetle (Coleoptera: Kateridae) in mid-Cretaceous Kachin amber (Myanmar). *Cretaceous Research* **106:** 104264.

Perrichot V, **Nel A**, **Néraudeau D**, **Lacau S**, **Guyot T. 2008.** New fossil ants in French Cretaceous amber (Hymenoptera: Formicidae). *Naturwissenschaften* **95:** 91–97.

Perrichot V, **Wang B**, **Barden P. 2020.** New remarkable hell ants (Formicidae: Haidomyrmecinae stat. nov.) from mid-Cretaceous amber of northern Myanmar. *Cretaceous Research* **109:** 104381.

de Queiroz K. 1998. The general lineage concept of species, species criteria, and the process of speciation: a conceptual unification and terminological recommendations. In: Raman S, ed. *Endless forms: species and speciation*. Oxford: Oxford University Press, 57–75.

de Queiroz K. 2007. Species concepts and species delimitation. *Systematic Biology* **56:** 879–886.

Richter A, **Keller RA**, **Rosumek FB**, **Economo EP**, **Hita Garcia F**, **Beutel RG. 2019.** The cephalic anatomy of workers of the ant species *Wasmannia affinis* (Formicidae, Hymenoptera, Insecta) and its evolutionary implications. *Arthropod Structure & Development* **49:** 26–49.

Richter A, **Hita Garcia F**, **Keller RA**, **Billen J**, **Economo EP**, **Beutel RG. 2020.** Comparative analysis of worker head anatomy of *Formica* and *Brachyponera* (Hymenoptera: Formicidae). *Arthropod Systematics & Phylogeny* **78:** 133–170.

Richter A, **Hita Garcia F**, **Keller RA**, **Billen J**, **Katzke J**, **Boudinot BE**, **Economo EP**, **Beutel RG. 2021.** The head anatomy of *Protanilla lini* (Hymenoptera: Formicidae: Leptanillinae), with a hypothesis of their mandibular movement. *Myrmecological News* **31:** 85–114.

Rolf DA. 1990. The evolution of flightlessness in insects. *Ecological Monographs* **60:** 389–421.

Shi C, **Yang Q**, **Shih C**, **Labandeira CC**, **Pang H**, **Ren D. 2020.** Cretaceous mantid lacewings with specialized raptorial forelegs illuminate modification of prey capture (Insecta: Neuroptera). *Zoological Journal of the Linnean Society* **190:** 1054–1070.

Storari AP, **Rodrigues T**, **Bantim RAM**, **Lima FJ**, **Saraiva AAF. 2021.** Mass mortality events of autochthonous faunas in a Lower Cretaceous Gondwanan Lagerstätte. *Scientific Reports* **11:** 6976.

Templeton AR. 1989. The meaning of species and speciation: a genetic perspective. In: Ereshefsky M, ed. *The units of evolution: essays on the nature of species*. Cambridge, London: MIT Press, 159–183.

Wagner GP. 2014. *Homology, genes, and evolutionary innovation*. Princeton: Princeton University Press, xiii + 478.

Wagner DL, **Liebherr JK. 1992.** Flightlessness in insects. *Trends in Ecology & Evolution* **7:** 216–220.

Wheeler DE. 1986. Developmental and physiological determinants of caste in social Hymenoptera: evolutionary implications. *American Naturalist* **128:** 13–34.

Wilson EO. 2008. One giant leap: how insects achieved altruism and colonial life. *BioScience* **58:** 17–25.

Wilson EO, **Brown WL Jr**. **1967.** Definition of †Sphecomyrminae, †*Sphecomyrma*, and †*S. freyi*. In: Wilson EO, Carpenter FM, Brown WL Jr., eds. The first Mesozoic ants, with the description of a new subfamily. *Psyche (Cambridge)* **74:** 6–10.

Wilson EO, **Carpenter FM**, **Brown WL Jr**. **1967a.** The first Mesozoic ants, with the description of a new subfamily. *Psyche (Cambridge)* **74:** 1–10.

Wilson EO, **Carpenter FM**, **Brown WL Jr**. **1967b.** The first Mesozoic ants. *Science* **157:** 1038–1040.

Wöhrl T, **Richter A**, **Guo S**, **Reinhardt L**, **Nowotny M**, **Blickhan R. 2021.** Comparative analysis of a geometric and an adhesive righting strategy against toppling in inclined hexapodal locomotion. *Journal of Experimental Biology* **224:** jeb242677.

Wu Q, **Yang H**, **Shih C**, **Ren D**, **Zhao Y**, **Gao T. 2021.** Vespids from the mid-Cretaceous with club-shaped antennae provide new evidence about the intrafamiliar relationships of Vespidae. *Zoological Journal of the Linnean Society* **193:** 217–229.

Zheng D, **Chang S-C**, **Perrichot V**, **Dutta S**, **Rudra A**, **Mu L**, **Kelly RS**, **Li S**, **Zhang Q**, **Zhang Q**, **Zhang Q**, **Wong J**, **Wang J**, **Wang H**, **Fang Y**, **Zhang H**, **Wang B. 2018.** A Late Cretaceous amber biota from central Myanmar. *Nature Communications* **9:** 3170.

Zuang Y, Ran H, Li X, Feng C, Liu Y. In press. A new species of the iron maiden ant based on an alate female from mid-Cretaceous Burmese amber (Hymenoptera: Formicidae: †Zigrasimecia). *Cretaceous Research*, 105056. doi:10.1016/j.cretres.2021.105056.

SUPPORTING INFORMATION

Additional Supporting Information may be found in the online version of this article at the publisher's web-site.

Figure S1. Scan parameters. Dataset 1. Morphometric definitions and data for specimens CASENT0741231–CASENT0741234. Dataset 2. Mesosomal development data. Complete habitus images of †*G. sternorhabda* paratype (CASENT0741234). A, dorsal view. B, ventral view.

Figure S2. Complete habitus images of †*G. sternorhabda* holotype (CASENT0741233). A, dorsal view. B, ventral view.

Figure S3. Complete habitus images of †*G. gracilis* non-type (CASENT0741232). A, dorsal view. B, ventral view.